

## 8. Peptides that React on Environmental Changes

Conformational transitions caused by subtle changes in the environment are discussed to be the most crucial event in the entire process of amyloidogenesis. In principle, many factors trigger structural conversions ranging from pH alterations to changes of the ionic strength, the presence of metal ions, elevated protein concentrations, oxidative stress, to the presence of a small quantity of a misfolded protein fragment (see section 2.2.2). During the work on this thesis, the two probably most interesting factors were selected: a changed pH value and the presence of transition metal ions. This section describes the development of pH or metal ion sensitive structural switches and their implementation in the previously described amyloid forming coiled coil model system.

### 8.1 *pH Switches*

For the generation of pH sensitivities, excessively charged domains that destabilize the helical structure itself without affecting both coiled coil recognition motifs have been incorporated. The validity of this approach was first proven by a design based on the ideally folded coiled coils VW01 and VW02. Subsequently, the developed functionalities have been incorporated into the amyloid forming coiled coil model peptide VW18.

#### 8.1.1 VW03

The design of peptide VW03 is based on the ideally folded coiled coils VW01 and VW02. Figure 8.1 shows the helical wheel diagram and the sequence of peptide VW03. Residues that form the two coiled coil recognition motifs have been kept unchanged so that a coiled coil structure can be adopted under certain conditions. Positions a and d are occupied by hydrophobic Leu residues to ensure an efficiently packed hydrophobic core, while positions e and g are equipped with complementarily charged Lys and Glu residues that exclusively form attractive interhelical Coulomb interactions in a parallel helix alignment. Thus, VW03 can inherently adopt an  $\alpha$ -helical coiled coil conformation.

As a pH sensitive functionality, Lys and Arg residues were incorporated at *heptad* repeat positions c and g, respectively. Furthermore, position b was substituted by Glu residues to at least partially obtain an equal distribution of positively and negatively charged amino acids. However, at acidic conditions, almost all charged side chains within the peptide strand are protonated. This yields a high accumulation of positive charges at one side of the helical cylinder (positions c, f, and g) that, due to strong intramolecular Coulomb repulsions, destabilize the helical structure. As a result, unfolding is expected at these conditions, which would therefore represent the “on” stage of the pH switch. In contrast, at neutral and slightly basic pH, positive and compensating negative charges are present which should facilitate the folding into a coiled coil structure. These conditions would therefore represent the “off” state of the pH switch.

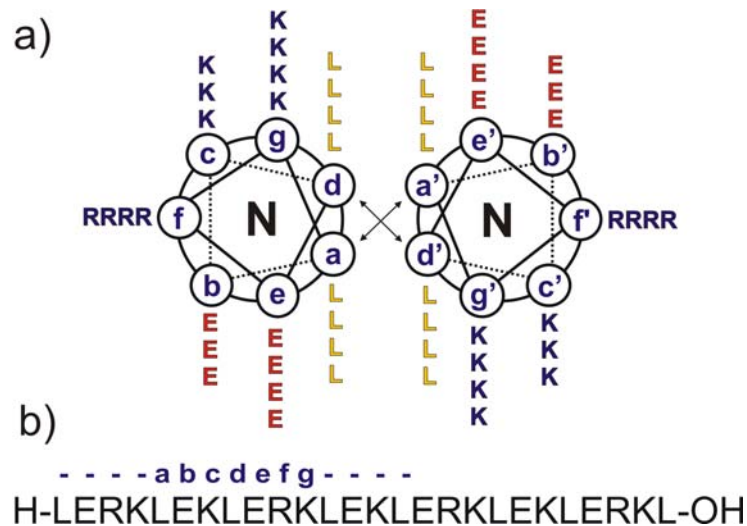


**Figure 8.1.** (a) Helical wheel diagram and (b) sequence of the pH sensitive peptide VW03.

Folding studies in a pH range from 4.0 to 8.0 confirmed the assumptions from the design. Figure 8.2 shows the CD spectra of VW03 at different pH values and a peptide concentration of approx. 250 $\mu$ M. Similar spectra have been obtained at lower concentrations. At pH 4.0 and 5.0 VW03 adopts a random coil conformation, while both, pH 7.4 and 8.0, yield typical  $\alpha$ -helical spectra. Therefore, the accumulation of positive charges at position c, f, and g of the *heptad* repeat results in destabilization of the  $\alpha$ -helical coiled coil structure, thus, providing a valuable design tool for the pH-directed disruption of helical structures.

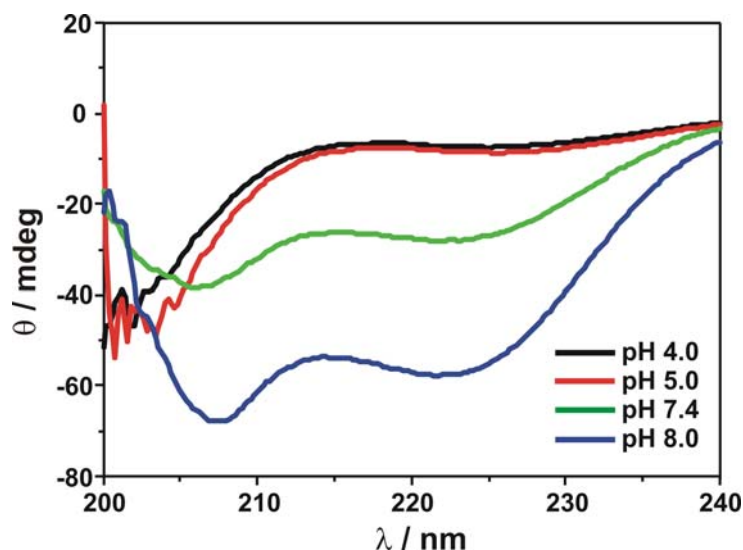


**Figure 8.2.** CD spectra of peptide VW03 at different pH values ( $c \sim 250\mu\text{M}$ , 10mM buffer, pH 4.0 - 5.0: acetate buffer, pH 7.4 – 8.0: Tris/HCl buffer).

Since VW03 is a direct descendant of VW01, thermal denaturation experiments have been performed to compare the coiled coil stabilities at pH 7.4 and 8.0 with those obtained for the ideally folded peptide. Table 8.1 shows the melting points of peptide VW03. Consistent with the observed folding behavior and the assumptions made from the design, these data clearly indicate an elevated stability with increasing pH value. However, VW03 exhibits similarly charged domains at both sides of the helix: (I) the extensively charged Lys / Arg surface formed by positions c, f, and g and (II) a smaller, negatively charged face formed by positions b and e. Therefore, repulsive electrostatic interactions between the Glu residues at neutral and slightly basic pH may also disturb the helical structure. Thus, it is not surprising that the overall stability of VW03 is perceptibly reduced in comparison to the ideally folded analog VW01, even at higher pH values.

**Table 8.1.** Melting temperatures of peptide VW03 at different pH values and GndHCl concentrations ( $c \sim 100\mu\text{M}$ , 10mM buffer, pH 7.4: Tris/HCl buffer, pH 8.0: phosphate buffer).

pH	Melting temperature in °C at			
	0 GndHCl	1M GndHCl	2M GndHCl	3M GndHCl
4.0	unfolded	unfolded	unfolded	unfolded
7.4	34.1	unfolded	unfolded	unfolded
8.0	58.5	40.3	unfolded	unfolded

### 8.1.2 VW04

In the next step, the concept of an excessively charged domain as a pH sensitive structural trigger was expanded by exchanging Lys and Arg with Glu and vice versa. Figure 8.3 shows a helical wheel diagram and the sequence of peptide VW04. As in the previously described peptide VW03, all positions that govern the coiled coil folding have been kept unchanged. Furthermore, the excessively charged domain at positions c, f, and g are now occupied by negatively charged Glu residues, while positions b and e are equipped with positively charged Lys residues. Hence, a complementary pH dependent folding behavior of peptide VW04 in comparison to VW03 is expected. Most of the Glu residues are protonated and uncharged at acidic conditions and should therefore enable a helical folding ("off" state), while charge repulsions between Glu residues at neutral and slightly basic pH should perceptibly disturb the helical conformation ("on" state).

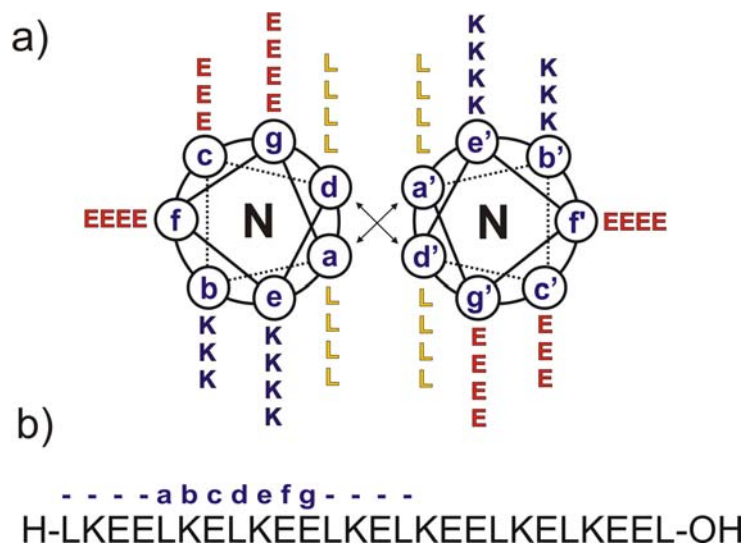


**Figure 8.3.** (a) Helical wheel diagram and (b) sequence of the pH sensitive peptide VW04.

Circular dichroism folding studies revealed that peptide VW04 indeed exhibits a complementary pH dependent folding behavior compared to VW03. Figure 8.4 shows the CD spectra of VW04 at different pH values and a peptide concentration of approx. 250  $\mu$ M. At acidic conditions typical  $\alpha$ -helical CD signatures are obtained, while random coil spectra are observed at neutral and slightly basic pH.

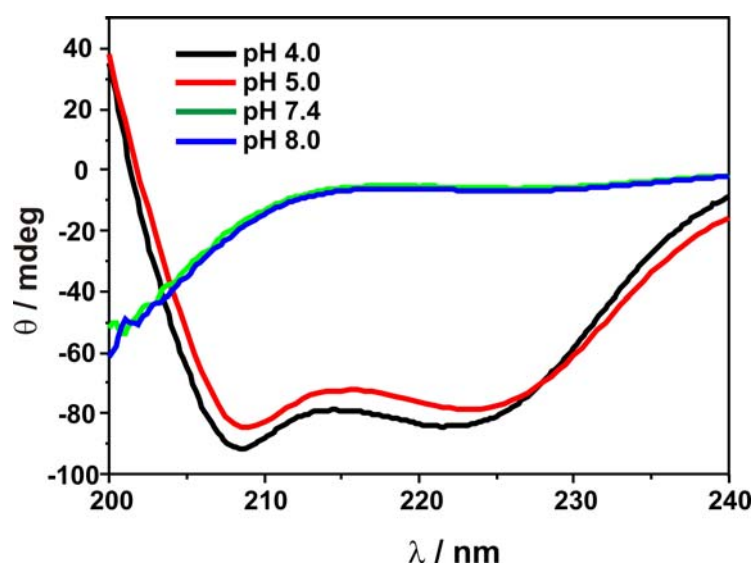


**Figure 8.4.** CD spectra of peptide VW04 at different pH values ( $c \sim 250\mu\text{M}$ , 10mM buffer, pH 4.0 - 5.0: acetate buffer, pH 7.4 – 8.0: Tris/HCl buffer).

In order to compare the stability of VW04 at acidic conditions with the stability of peptide VW03 at neutral and slightly basic conditions, thermal denaturation profiles were recorded. **Table 8.2** shows the calculated melting points of peptide VW04 at pH 4.0. Surprisingly, these data clearly indicate that the  $\alpha$ -helical coiled coil form of VW04 at acidic pH exhibits a stability which is comparable or even higher than that obtained for VW01 at similar conditions. This unexpectedly high stability may have resulted from the unusual helix stabilizing properties of protonated Glu residues, which was already discussed for peptide VW18 (see section 7.2.6).<sup>224-226</sup> Thus, it can be concluded that peptides VW03 and VW04 exhibit a complementary pH dependent conformational preference. However, a direct comparison should be avoided since the detailed intrinsic differences between Glu and Lys, i.e., the distinct side chain lengths and their consequences on the pK value, cannot be sufficiently explained by the term complementary.

**Table 8.2.** Melting temperatures of peptide VW04 at different pH values and GndHCl concentrations ( $c \sim 100\mu\text{M}$ , 10mM buffer, pH 7.4: Tris/HCl buffer, pH 8.0: phosphate buffer).

pH	Melting temperature in °C at			
	0 GndHCl	1M GndHCl	2M GndHCl	3M GndHCl
4.0	>50% folded	63.6	52.0	30.6
7.4	unfolded	unfolded	unfolded	unfolded
8.0	unfolded	unfolded	unfolded	unfolded



Figure 8.5 shows the sequence of peptide VW19 as a helical wheel model and as an extended parallel and antiparallel  $\beta$ -sheet aligned in a zigzag fashion. In principle, the design can be explained with three general features: (I) As in all previously described peptides, the two coiled coil recognition motifs have been designed for perfect complementarity to maintain the ability of a stable  $\alpha$ -helical coiled coil folding, which is a central requirement of the design. Positions a and d are exclusively occupied by hydrophobic Leucine, while residues at *heptad* repeat positions e, g, and e', g', respectively, were arranged to solely form attractive electrostatic interactions in a parallel helix alignment. (II) Lysine residues in b and f in combination with position e form a large excessively charged domain, analogous to the pH-switch developed in peptide VW03. At acidic conditions, an excess of positive charges at one side of the helical surface results in a destabilization and unfolding of the  $\alpha$ -helix as shown in the previous subsections. (III) According to the optimized amyloid forming coiled coil model VW18, three Val residues were incorporated at the solvent exposed positions 13 (b), 14 (c), and 3 (f) in order to make the system prone to  $\beta$ -sheet formation.

The folding behavior of peptide VW19 has been extensively studied by various bioanalytical and biophysical techniques.<sup>221,227-229</sup> For clarity reasons, only selected data are presented in the following. Further information can be obtained elsewhere.<sup>221,227-229</sup> Not surprisingly, the peptide concentration was shown to play a significant role for the adopted conformation. At pH 4.0 as well as 7.4, exclusively random coil CD spectra have been obtained for concentrations below a threshold of approx. 300 $\mu$ M. These spectra were invariable for the entire observation period of one week. Figure 8.6 a exemplarily shows the CD spectra of a 250 $\mu$ M VW19 solution at pH 4.0 and different incubation times. Furthermore, cryo-TEM measurements have been performed to characterize peptide and aggregate morphology. Figure 8.6 b shows the obtained cryo-TEM micrograph of a 250 $\mu$ M VW19 solution at pH 4.0 and an incubation time of 6 days. For an unfolded, single solvated 26 residue peptide molecule (with an idealized spherical shape and a partial specific volume of 0.744cm<sup>3</sup>/g), a theoretical diameter of about 2nm can be estimated. Cryo-TEM revealed ensembles of very small peptide particles with a typical size in the range of 2.5-3.5nm, which is in good agreement with the theoretical estimation. The exact particle shape cannot be specified due to the small size. However, the size homogeneity points to a nearly globular state. Thus, in a pH range from 4.0 to 7.4, VW19 doubtlessly remains unfolded at concentrations below 300 $\mu$ M.

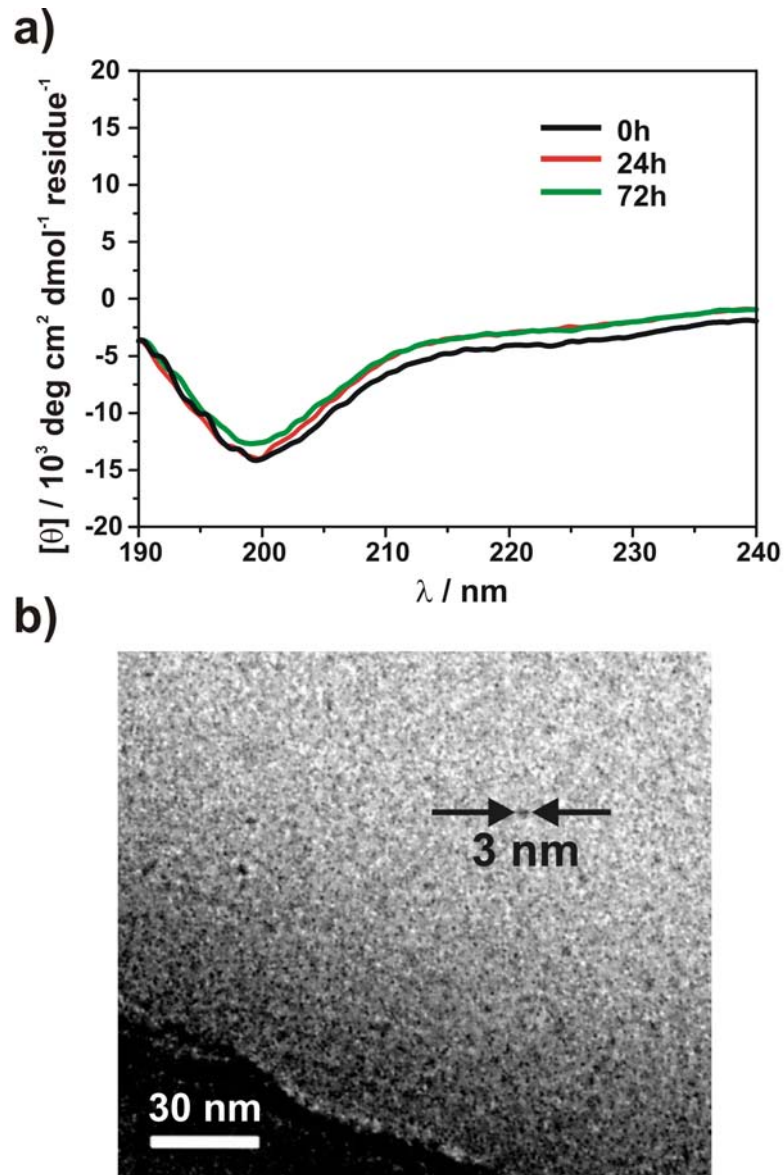


**Figure 8.6.** (a) Time dependently recorded CD spectra of peptide VW19 at pH 4.0 and a peptide concentration below  $300\mu\text{M}$  ( $c = 250\mu\text{M}$ , 10mM acetate buffer, pH 4.0). (b) Cryo-TEM micrograph of  $250\mu\text{M}$  VW19 at pH 4.0 after 6 days of incubation.

At higher concentrations, distinct differences in the folding behavior of VW19 have been observed for acidic and neutral pH values. Increasing the peptide concentration above  $300\mu\text{M}$  at pH 4.0 induces the transition to a  $\beta$ -sheet conformation, as indicated by the appearance of a typical minimum at 216nm within 3 days (Figure 8.7 a). Cryo-TEM images of “matured” solutions furthermore revealed regular fibrous aggregates in the order of microns in length (Figure 8.7 b). Those aggregates exhibit a characteristic

helically twisted ribbon morphology, similar to those that have been reported for other amyloid forming systems.<sup>123</sup> Additionally, a peptide-peptide periodicity of 0.47nm measured by electron diffraction supports the evidence of a cross  $\beta$ -structure organization within the ribbons<sup>227</sup> and Congo red staining experiment further confirmed the presence of amyloids.<sup>229</sup> Though, peptide VW19 beyond doubt forms amyloids at pH 4.0 and concentrations below 300 $\mu$ M, i.e., conditions representing the “on” state of the pH switch.

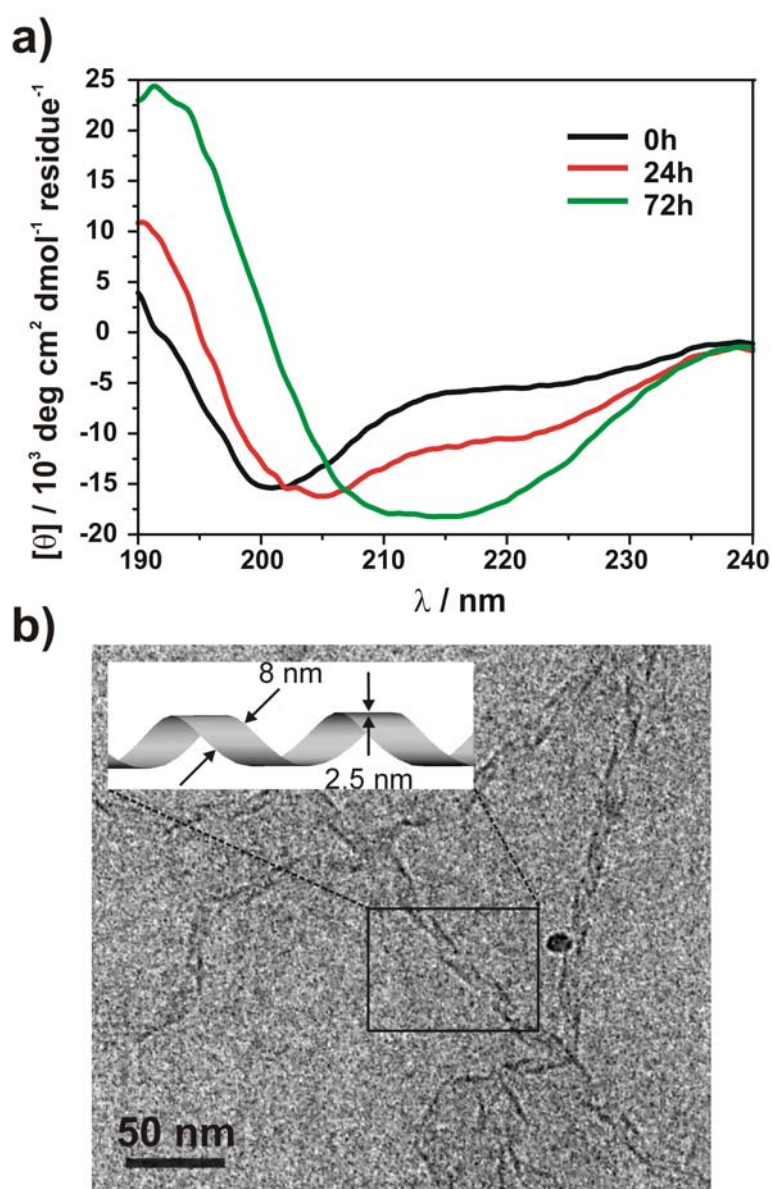


**Figure 8.7.** (a) Time dependently recorded CD spectra of peptide VW19 at pH 4.0 and a peptide concentration above 300 $\mu$ M ( $c = 600\mu\text{M}$ , 10mM acetate buffer, pH 4.0). (b) Cryo-TEM micrograph of 600 $\mu$ M VW19 at pH 4.0 after 6 days of incubation.

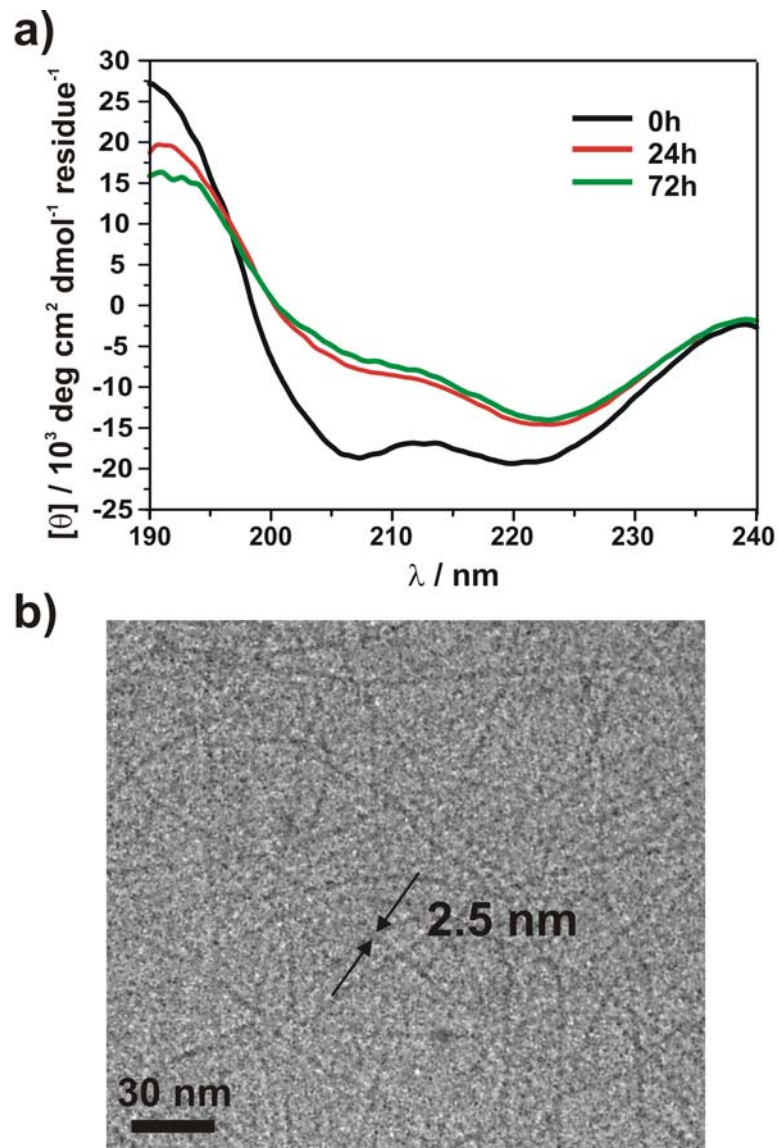


**Figure 8.8.** (a) Time dependently recorded CD spectra of peptide VW19 at pH 7.4 and a peptide concentration above  $300\mu\text{M}$  ( $c = 600\mu\text{M}$ , 10mM Tris / HCl buffer, pH 7.4). (b) Cryo-TEM micrograph of  $600\mu\text{M}$  VW19 at pH 7.4 after 6 days of incubation.

The dimensions determined from the cryo-TEM micrographs lead to the assumption that the helical ribbons consists of fully extended  $\beta$ -sheets which form typical double-layered fibrils. The ribbon width of  $8 \pm 2\text{nm}$  is in good agreement with a calculated length of 9.1nm for the extended 26-residue peptide VW19. Moreover, the ribbon thickness of about 2.5nm estimated from the cryo-TEM micrographs suggests the double-layered packing of peptide molecules. Further cryo-TEM measurements on VW19 and related peptides, however, revealed the presence of protofilaments with a perceptibly smaller width of approx. 3.5nm.<sup>228</sup> These data are in contradiction to the extended  $\beta$ -strand model. Since, the internal protofilament structure of VW19 has not yet been

characterized sufficiently, further structural hypotheses would be highly speculative. In principle, most of the proposed structural models discussed in section 2.1.2 are conceivable possibilities. Solid state NMR experiments are currently under progression to clarify the molecular arrangement within the protofilaments. Additionally, proline scanning analysis should provide valuable information on the presence and location of possible turn or loop segments.

In contrast to acidic conditions, VW19 adopts an  $\alpha$ -helical conformation at pH 7.4 and concentrations above 300 $\mu$ M as indicated by the occurrence of two characteristic minima in the CD spectra. Higher concentrated samples show decreasing ellipticities at 208nm over several days (Figure 8.8 a), which point to gradual molecular rearrangements.<sup>144</sup> Cryo-TEM images reveal extended fibers with total lengths in the micrometer range and a uniform diameter of  $2.5 \pm 0.3$ nm, regardless of the peptide concentration (Figure 8.8 b). According to the characteristic CD spectrum and the unusually high concentration, an  $\alpha$ -helical coiled coil organization of the peptide within the fibers can be assumed. Similar  $\alpha$ -helical fibers derived from coiled coil peptides have been reported in the literature (see section 3.4.2).<sup>86,125,144-148</sup> Figure 8.9 shows the structural model of a five-stranded  $\alpha$ -helical fiber containing 34 residue coiled coil peptides.<sup>148</sup>

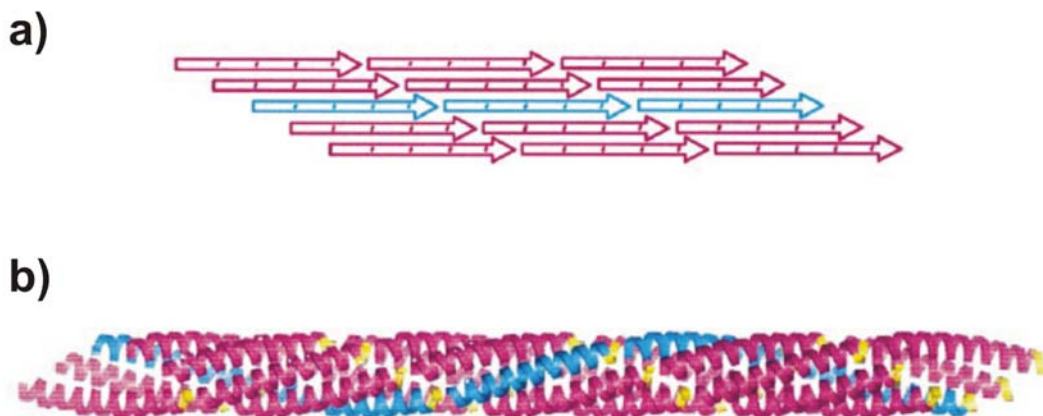


**Figure 8.9.** Structural model of a pentameric  $\alpha$ -helical fiber. (a) Two-dimensional schematic representation of a fibril with staggered  $\alpha$ -helices.  $\alpha$ -Helices are shown as arrows with cross-lines indicating the heptad repeats. (b) Structural model of an  $\alpha$ -helical five-stranded fibril containing 34-residue peptides. Each strand is formed by the  $\alpha$ -helices aligned head-to-tail (one strand is shown in blue, N-termini are in yellow). The strands are wrapped around the coiled coil axis in a left-handed superhelix with parameters similar to those of conventional pentameric coiled coils (according to S. A. Potekhin et al.).<sup>148</sup>

The estimated diameter of VW19  $\alpha$ -fibrils is in good agreement with data reported in the literature and points to a four- or five-stranded assembly.<sup>148</sup> However, to establish a quantitative structure model of VW19  $\alpha$ -fibrils, more experimental data from X-ray diffraction or solid-state NMR experiments are needed. Regrettably, both techniques require preliminary sample enrichment procedures which turned out to be the most critical issue for these experiments. In contrast to the expectations, conventional ultra centrifugation yielded amyloid formation for VW19 also at neutral pH. This conformational transition presumably results from extraordinary high local concentrations which might induce structural conversions even at conditions where amyloids are usually not observed. Also slow sample drying approaches to enable X-ray diffraction experiments failed, because only insufficient concentration enhancement was obtained. A further development of the sample enrichment procedure is a basic necessity for detailed structural investigations.

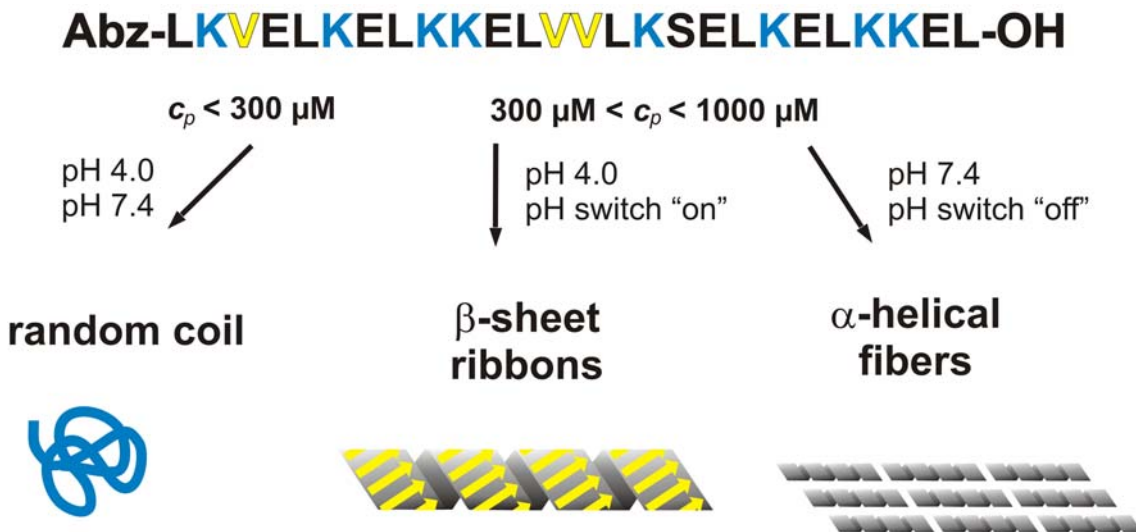


**Figure 8.10.** Graphical summary of VW19's pH and concentration controllable folding behaviour.

In conclusion, combining the design principles of the amyloid forming coiled coil VW18 and the pH sensitive peptide VW03 indeed yielded a model peptide with concentration and pH controllable amyloid formation properties. Figure 8.10 shows a graphical summary of the observed folding behavior. Concentrations below a threshold of approx. 300 $\mu\text{M}$  yielded unfolding, while higher concentrated samples were shown to either form amyloid fibrils at acidic conditions ("on" state of the pH switch) or  $\alpha$ -helical fibers at neutral pH ("off" state of the pH switch). From a more general viewpoint these data impres-

sively highlight the paramount importance of a changed environment on peptide folding and amyloid formation. Marginally altered conditions resulted in the formation of three completely different conformations without changes in the primary structure.

### 8.1.4 Continuative VW19 Related Peptides

The findings on peptide VW19 made it interesting to see how a direct Lys→Glu exchange at position f of the *heptad* repeat affects folding and amyloid formation. In principle, an analogous complementary behavior as observed for VW03 and VW04 would be expected. Consequently, further investigations on VW19 related peptides were carried out in our group.<sup>223,228</sup> The direct Lys→Glu exchange at *heptad* repeat position f yielded peptide RR01, which indeed exhibits a reverse pH dependence of folding and, thus, intriguingly confirms the applied design principles (Figure 8.11). Detailed information on these experiments can be obtained elsewhere.<sup>223,228</sup>

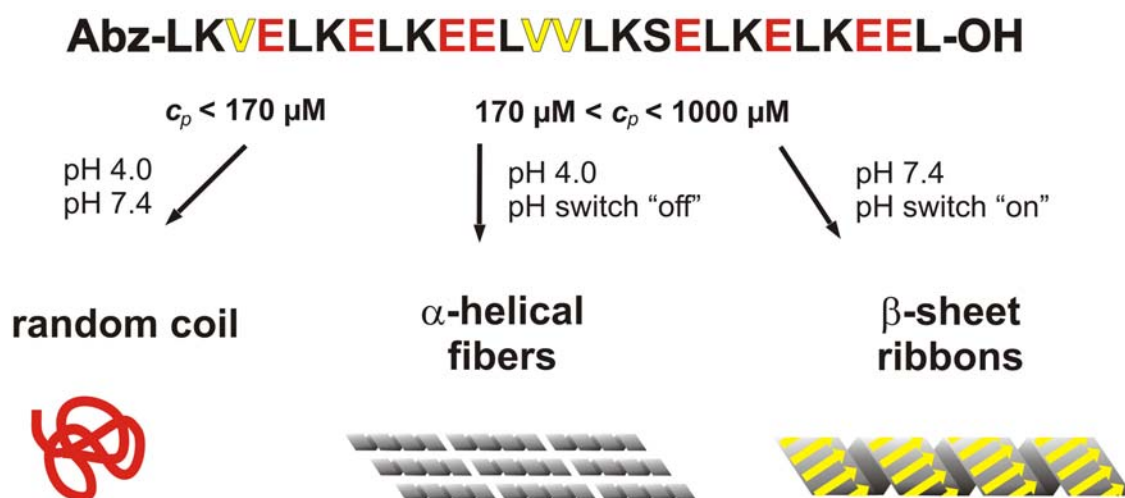


**Figure 8.11.** Graphical summary of RR01's pH and concentration controllable folding behaviour.<sup>223,228</sup>

## 8.2 Metal Ion Coordination as Structural Trigger

The second environmental factor which was studied extensively on basis of the presented amyloid forming coiled coil system is the presence of transition metal ions. Due to the naturally high concentration of heavy metal ions in the brain and their importance in the context of neurodegenerative diseases, the influence of metallochemical reactions on amyloid formation processes has drawn increased attention in recent years.<sup>69-71</sup> In general, two distinctly different classes of metal dependent reactions are found for neurodegenerative diseases. Firstly, there are metal-protein association processes which lead to protein aggregation and amyloid formation. These reactions can involve redox-inactive metal ions such as  $Zn^{2+}$  as well as redox-active metal ions such as  $Cu^{2+}$  and  $Fe^{3+}$ . Secondly, there are transition metal-catalyzed protein oxidation processes that lead to protein damage and denaturation. These reactions exclusively involve redox-active metal ions such as  $Cu^{2+}$ ,  $Fe^{3+}$  or  $Mn^{2+}$ .<sup>69,70</sup>

The research presented here is focused on investigations regarding the first class of metal dependent reactions. To study the impact of metallochemical reactions on protein folding, aggregation, and amyloid association, several coiled coil based amyloid forming model peptides with transition metal ion sensitive functionalities have been designed and characterized. These results are summarized in the following subsections.

### 8.2.1 Design Concepts of Metal Ion Sensitive Functionalities

In recent years, an enormous effort has been spent on investigations and experiments regarding the metal binding properties of naturally occurring amyloid forming proteins and their segments.<sup>69,71</sup> Curiously, no *de novo* design approaches addressing this issue have been published to date. Nevertheless, many strategies for the implementation of metal ion dependent structural switches in peptides and proteins, which are not related to amyloid formation, have been reported.<sup>108,230,231</sup> In an early work the Kelly lab published a scaffold based system that adopted a  $\beta$ -hairpin-like conformation in the presence of  $Cu^{2+}$ .<sup>117</sup> Furthermore, the Schneider group described the rational design of an  $As^{3+}$ -binding  $\beta$ -hairpin peptide.<sup>232</sup>

Additionally, a manifold of design approaches based on the  $\alpha$ -helical coiled coil folding motif have been reported. Using different methodologies, the groups of Woolfson and Kuhlman simultaneously described the design principles of artificial coiled coil based model systems that adopt the unique conformation of a zinc-finger protein upon zinc coordination.<sup>67,233</sup> Furthermore, various natural and non-natural metal binding residues have been incorporated at different positions within the coiled coil *heptad* repeat. Metal binding to artificial ligands placed at the terminal end of peptide strands demonstrated the potential to direct the assembly of single molecules into a trimeric coiled coil.<sup>234</sup> Moreover, ligands placed at the solvent exposed b, c, and f positions revealed the ability of metal coordination to control the coiled coil oligomerization state.<sup>235</sup> Similar effects have been observed for peptides containing metal binding Cys residues at the interior hydrophobic core positions a and d.<sup>236-239</sup> Additionally, Hodges and co-workers reported the metal ion induced  $\alpha$ -helical folding of a *de novo* designed peptide that contained non-natural  $\gamma$ -carboxyglutamic acid residues at e and g positions.<sup>240</sup>

Most of the literature-described coiled coil based approaches by design aimed a stability enhancement of the helical conformation upon the coordination of metal ions. With a focus on amyloid formation processes, however, both, metal directed helix stabilization and helix destabilization may contribute significantly. Thus, the so called *i,i+2* and *i,i+4* strategy which was first introduced by Sugiura and co-workers was followed.<sup>241</sup> In this study the impact of  $\text{Fe}^{3+}$  binding to non-natural Ida residues which were incorporated at different positions within the *heptad* repeat was investigated.<sup>241</sup> Furthermore, the same group used the *i,i+2* approach for the construction of a peptide based metal-gated ion channel.<sup>242</sup>

Figure 8.12 shows the basic idea behind the *i,i+2* and *i,i+4* approach. Placing a coordinating residue at the *i* and *i+2* positions within the *heptad* repeat yields a strong distortion of the peptide backbone upon metal binding that results in a destabilization of the helical structure and consecutive unfolding. Although it was not considered in the work of the Sugiura group,<sup>241</sup> *i* and *i+2* substitutions might furthermore be amyloid inducing or stabilizing since both metal binding residues are presented at the same side of the alternating  $\beta$ -sheet and can therefore be easily accessed by metal ions. Substitution of histidine at positions *i* and *i+4* yields a contrary behavior. Here, both residues are in close spatial proximity in a helical folding. Metal coordination therefore results in a stabilization of the helical conformation. Analogous effects have been observed for modifications on the naturally occurring coiled coil GCN4.<sup>243</sup>

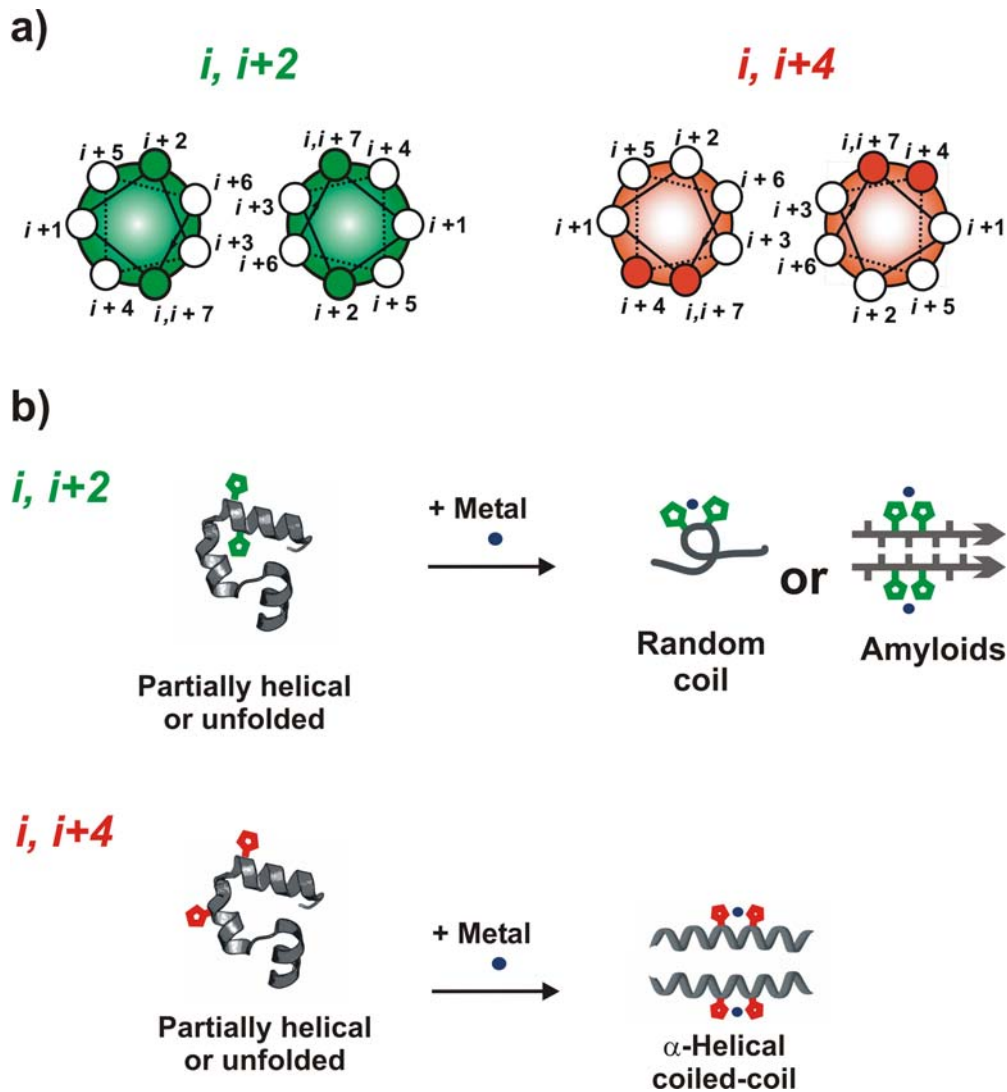


**Figure 8.12.** The  $i, i+2$  and  $i, i+4$  strategy. (a) Helical wheel diagram showing the position of metal ion binding residues incorporated at positions  $i, i+2$  as well as  $i, i+4$  within the coiled coil heptad repeat. (b) Expected folding behaviour.

Since the structure-inducing factor of the  $i, i+2$  and  $i, i+4$  strategy was shown to be the position of the coordinating residues relative towards each other and not their specific metal binding characteristic, this approach is a suitable tool for application in amyloid forming model systems.<sup>241</sup> In contrast to the primary study,<sup>241</sup> histidine was used as metal coordinating residue to make the model as close to nature as possible. At pH values above the  $pK_a$  of approx. 6.0, His imidazole side chains are efficient ligands for transition metal ions and have furthermore been shown to be the major component governing the metal binding properties in most of the naturally occurring amyloid form-

ing proteins such as A $\beta$  and the prion proteins. Combining the strategies of His incorporation at either the  $i$  and  $i+2$  or  $i$  and  $i+4$  positions with features from the amyloid forming coiled coil model VW18 should, thus, yield a model peptide system with amyloid formation properties that strongly depend on the presence of transition metal ions.

### 8.2.2 VW15

Prior to the application of the  $i,i+2$  and  $i,i+4$  strategy the metal ion dependent structure formation of a VW11 based, His-rich peptide denoted VW15 was investigated. As the name implies, this peptide has been designed and characterized before the basic amyloid forming coiled coil model VW18 was investigated. Thus, the results presented here provide a basis for the further metal ion dependent structural studies but can, because of extensive differences in the primary structure, only be somewhat compared with the other peptides presented in this section.

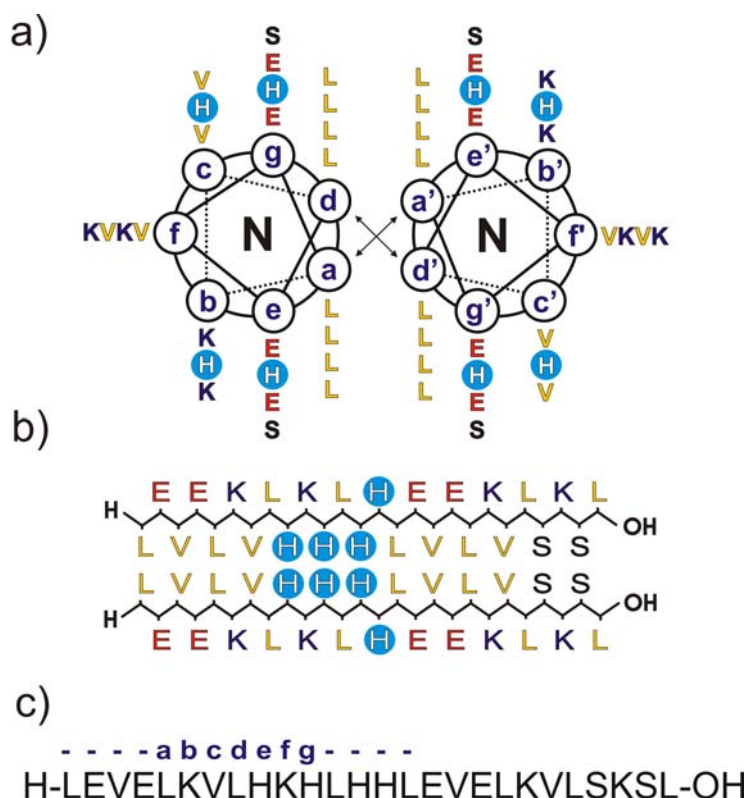


**Figure 8.13.** (a) Helical wheel diagram, (b) zigzag model of a parallel  $\beta$ -sheet, and (c) sequence of peptide VW15. His residues are depicted in light blue.

Figure 8.13 shows the sequence of peptide VW15 as a helical wheel model and as an extended parallel  $\beta$ -sheet aligned in a zigzag fashion. In contrast to VW11, peptide VW15 contains four metal coordinating His residues at b, c, e, and g position of the coiled coil *heptad* repeat. Consequently, VW15 simultaneously fulfils the design requirements of both an  $i,i+2$  as well as  $i,i+4$  incorporation of metal binding residues. In a helical folding two His residues would be aligned in close spatial proximity on both sides of the helical cylinder. On the other hand, three histidines would be arranged adjacently within the hydrophobic core in an amphiphilic  $\beta$ -sheet conformation. As a result, peptide VW15 intrinsically facilitates and stabilizes both the  $\alpha$ -helical as well as the  $\beta$ -sheet structure. Sequentially, the specific binding characteristics of the metal ion and underlying peptide-metal stoichiometry are supposed to dictate the resulting peptide conformation.

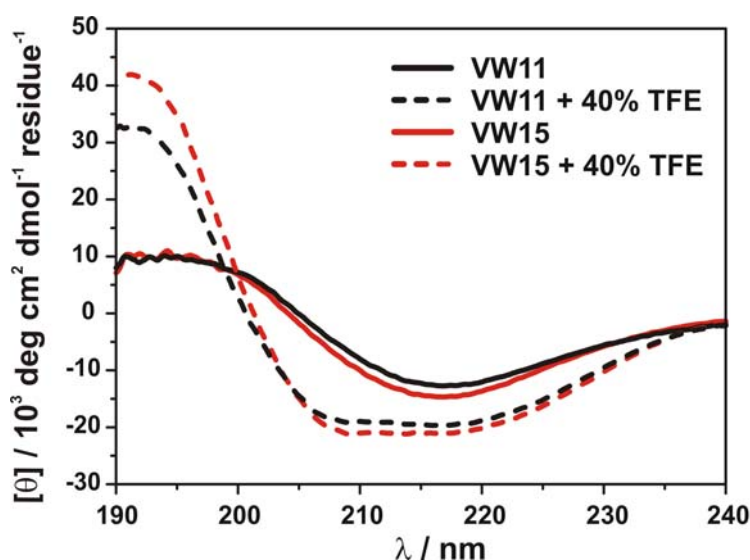


**Figure 8.14.** CD spectra of peptide VW11Abz and VW15 in the absence (solid line) or in presence (dashed line) of 40% TFE ( $c = 100\mu\text{M}$ , 10mM Tris / HCl, pH 7.4).

In order to compare the folding behavior of VW15 and its non-His containing analogue VW11Abz, both peptides have been studied simultaneously by CD spectroscopy at pH 7.4. Lower pH values were not studied, because His imidazole side chains are protonated at these conditions and would consequently be incapable for coordinating metal ions efficiently. At aqueous conditions and a peptide concentration of  $100\mu\text{M}$ , VW15 adopts a clear  $\beta$ -sheet conformation with CD signatures similar to those obtained for VW11 (Figure 8.14). Analogous spectra have been obtained for lower concentrations

up to 25 $\mu$ M (data not shown).<sup>244</sup> Thus, a comparable  $\beta$ -sheet formation propensity can be assumed for both peptides. Subsequently, different amounts of TFE have been employed to generate solvent conditions which are known to promote an  $\alpha$ -helical structure.<sup>245</sup> The spectra acquired (data not shown) clearly show that under the influence of TFE the general propensity to switch from a  $\beta$ -sheet to an  $\alpha$ -helical conformation is analogous for both peptides.<sup>244</sup> Since both peptides adopt a helical conformation at 40% TFE (Figure 8.14), these conditions were chosen for further investigation of the metal dependent folding behavior.

As expected, addition of one equivalent of  $\text{Cu}^{2+}$  as well as  $\text{Zn}^{2+}$  to a 100 $\mu$ M solution of the His-free peptide VW11Abz, did not result in any significant change of its secondary structure (Figure 8.15). In contrast, the addition of  $\text{Cu}^{2+}$  and  $\text{Zn}^{2+}$  ions, respectively, had a strong impact on the folding of peptide VW15, which exhibited a vigorous switch from the mainly  $\alpha$ -helical structure to a conformation that is rich in  $\beta$ -sheet (Figure 8.16 and Figure 8.17). Based on this observation, the metal scavenger EDTA was applied to analyze a potential reversibility of the conformational transition. The addition of equimolar amounts of EDTA (Figure 8.16 and Figure 8.17) resulted in a complete recovery of the primarily helical structure. Thus, the structural transition can be reversed by simply capturing the  $\beta$ -sheet-inducing metal ions and, as a result, can be arbitrarily shifted in either direction.

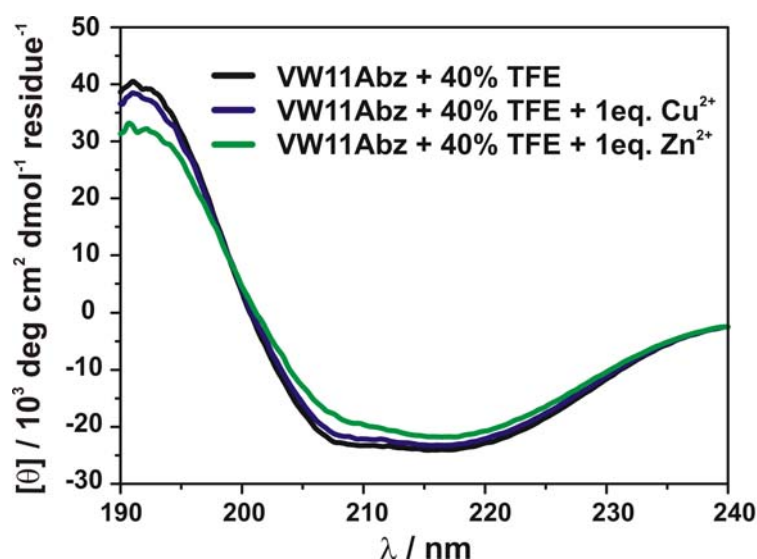


**Figure 8.15.** CD spectra of peptide VW11Abz in 40%TFE in presence of 1eq.  $\text{Cu}^{2+}$  or  $\text{Zn}^{2+}$  ( $c = 100\mu\text{M}$ , 10mM Tris / HCl, pH 7.4).

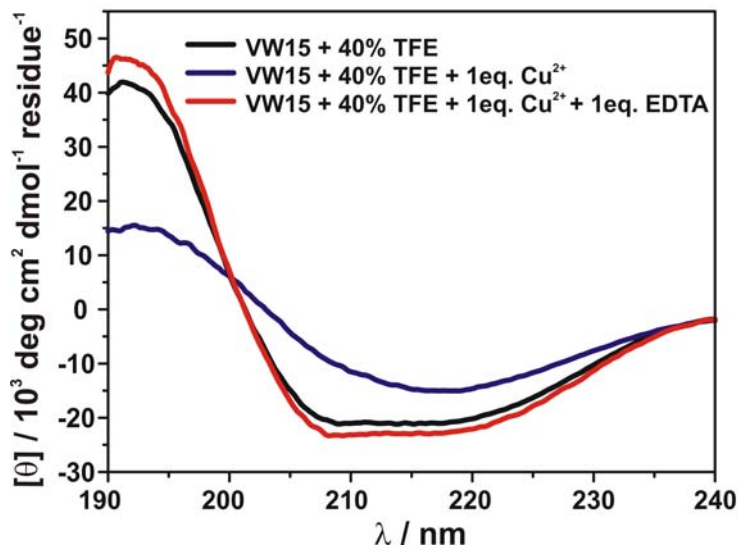


**Figure 8.16.** CD spectra of peptide VW15 in 40%TFE, in 40%TFE and 1eq.  $\text{Cu}^{2+}$  and in 40% TFE in presence of 1eq.  $\text{Cu}^{2+}$  and 1eq. EDTA ( $c = 100\mu\text{M}$ , 10mM Tris / HCl, pH 7.4, 40% TFE).

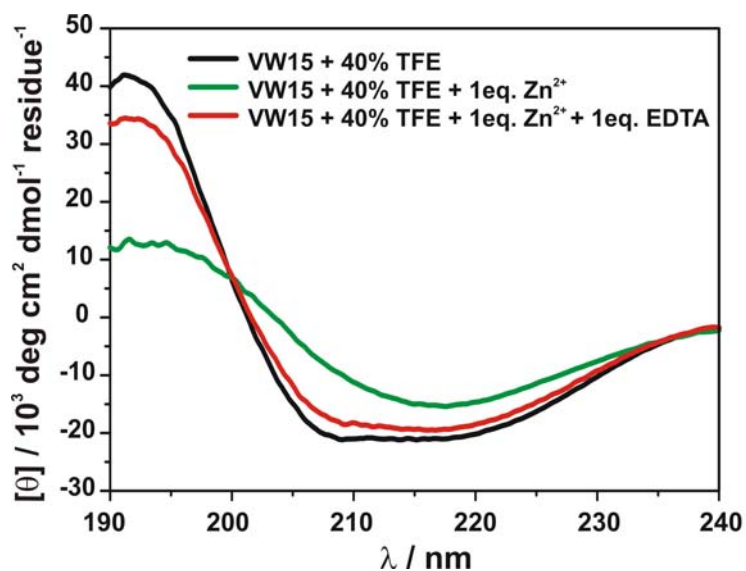


**Figure 8.17.** CD spectra of peptide VW15 in 40%TFE, in 40%TFE and 1eq.  $\text{Zn}^{2+}$  and in 40% TFE in presence of 1eq.  $\text{Zn}^{2+}$  and 1eq. EDTA ( $c = 100\mu\text{M}$ , 10mM Tris / HCl, pH 7.4, 40% TFE).

Metal ion titration experiments were performed to further confirm the structure inducing effect of the peptide-metal coordination event. Therefore, the  $[\theta]_{208}$  values at different  $\text{Cu}^{2+}$  or  $\text{Zn}^{2+}$  concentrations were recorded by CD spectroscopy.<sup>244</sup> Figure 8.18 shows the obtained profile for the VW15- $\text{Zn}^{2+}$  titration. For both  $\text{Cu}^{2+}$  (data not shown) as well as  $\text{Zn}^{2+}$  (Figure 8.18), a typical single exponential increase of the ellipticity at 208nm was found for increasing metal concentrations. This points to a specific metal ion dependent  $\alpha \rightarrow \beta$  structural transition process. Moreover, these data provide evidence that the peptide-metal complex exhibits a 2:1 stoichiometry (Figure 8.18).

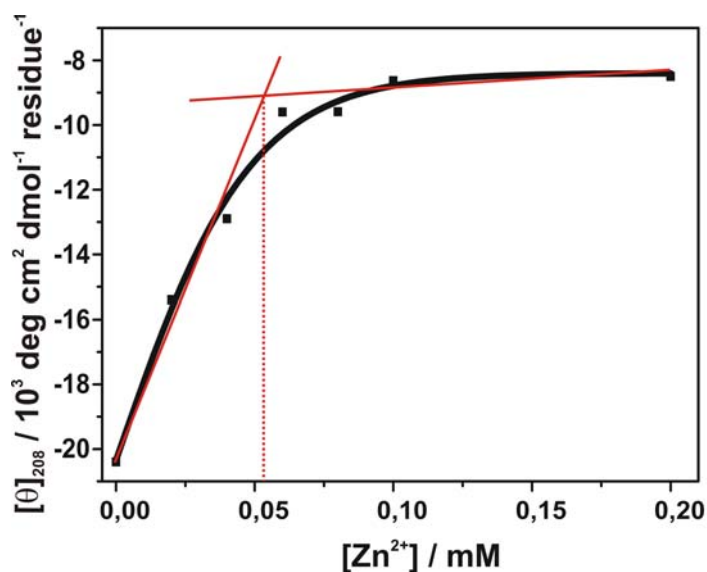


**Figure 8.18.** CD spectroscopic  $\text{Zn}^{2+}$  titration of peptide VW15 in 40% TFE ( $c = 100 \mu\text{M}$ , 10mM Tris / HCl, pH 7.4). The intersection point of the idealized lines (red) indicates an underlying peptide-metal stoichiometry of 2:1.

Taken together, these results highlight the enormous potential of metal ion coordination as a trigger for conformational changes. Both  $\text{Cu}^{2+}$  as well as  $\text{Zn}^{2+}$  initiate a structural transition from  $\alpha$ -helix to  $\beta$ -sheet and the estimated binding stoichiometry of 2:1 implies that each metal ion binds two peptide strands. It can therefore be assumed that the increased peptide content in the peptide-metal complex facilitates the formation of oligomeric, amphiphilic  $\beta$ -sheets and, thus, acts structure inducing. More experimental data are necessary to validate this assumption. Moreover, the presented results highlight the importance of His as efficient metal coordinating residue. Although not only the His side chains can be involved in metal ion binding but also the backbone NH and CO, the inability of the non-His-containing peptide VW11Abz to change its conformation upon metal addition reveals the importance of His as a major complexing component.

The unusually high content of TFE hampers any comparison with naturally occurring systems. These experiments, however, are merely preliminary investigations to establish a basis for other His containing peptides which exhibit structural conversions at native-like aqueous conditions.

### 8.2.3 VW23 and VW24

In order to prove the validity of the  $i,i+2$  and  $i,i+4$  strategy for the design, peptides VW23 and VW24 were designed.<sup>246</sup> Both sequences are His containing derivatives of VW17 and therefore no amyloid formation is expected (see section 7.2.5). Figure 8.19 shows the sequence of VW23 and VW24 as a helical wheel model and as an extended parallel and antiparallel  $\beta$ -sheet aligned in a zigzag fashion.

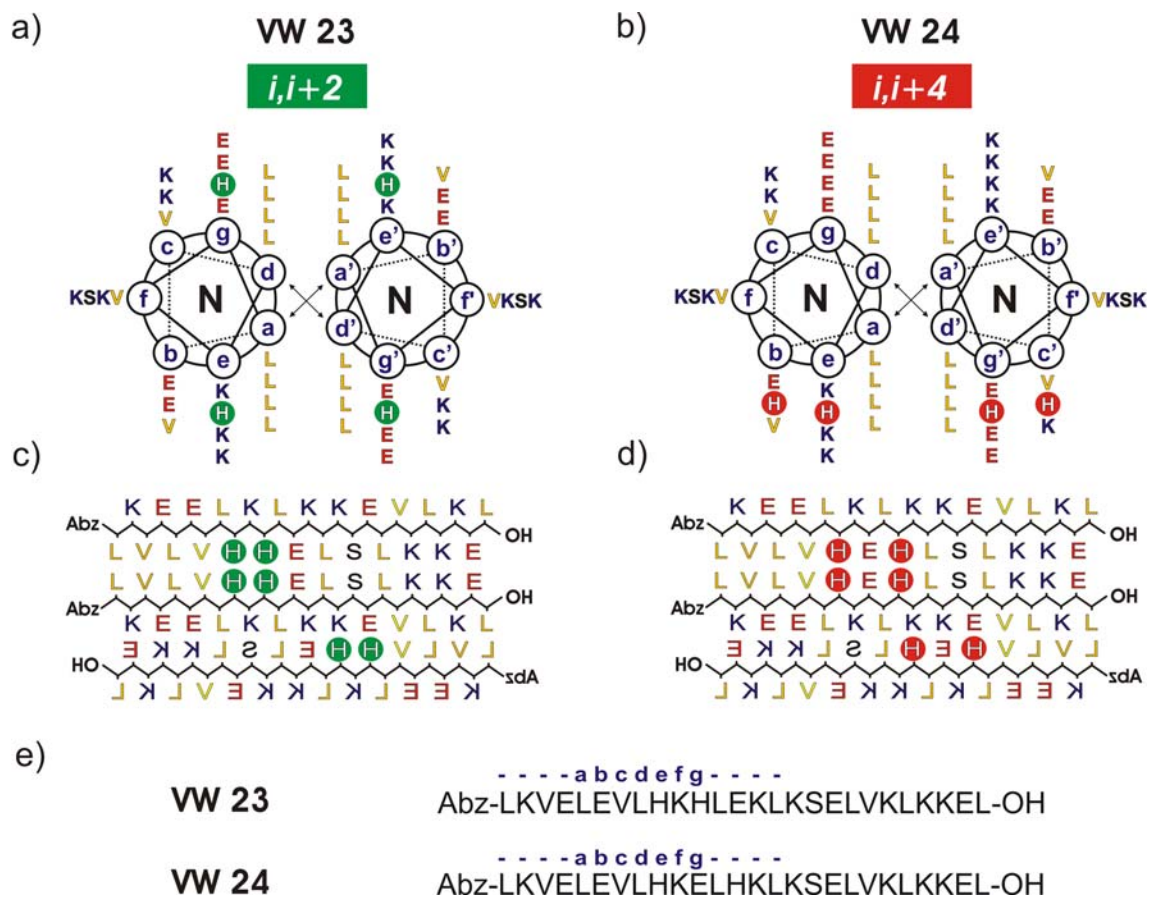


**Figure 8.19.** (a and b) Helical wheel diagram, (c and d) zigzag model of a parallel and an antiparallel  $\beta$ -sheet, as well as (e) sequence of peptides VW23 and VW24.

To maximize the impact of metal binding on the adopted conformation, His residues were placed at central positions within the sequence. It was necessary to rearrange two of the Val residues at the solvent exposed *heptad* repeat positions from 13 (b) and 14 (c) to 20 (b) and 7 (c), respectively. During the work on this thesis it turned out that this modification has a tremendous effect on the overall amyloid formation properties of the model system. Further discussions addressing this issue are presented in the following sections. However, VW23 contains two His residues at *i* and *i*+2 positions, while VW24 was modified with His at the *i* and *i*+4 positions. Consequently, metal ion induced unfolding is expected for VW23 whereas VW24 is expected to exhibit a perceptible stabilization of the helical conformation upon metal binding.

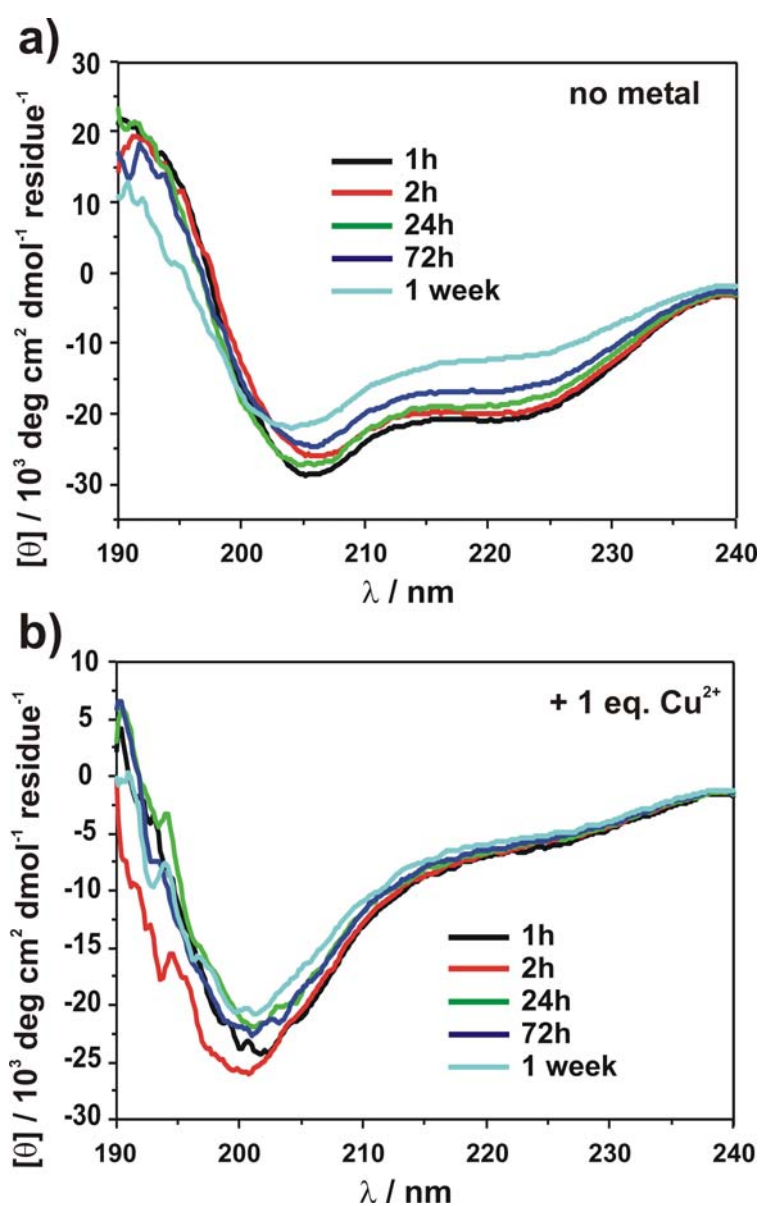


**Figure 8.20.** (a) CD spectra of peptide VW23 (*i,i*+2) in the absence of metal ions and (b) in presence of 1 eq.  $\text{Cu}^{2+}$  ( $c = 100\mu\text{M}$ , 10mM Tris / HCl, pH 7.4).

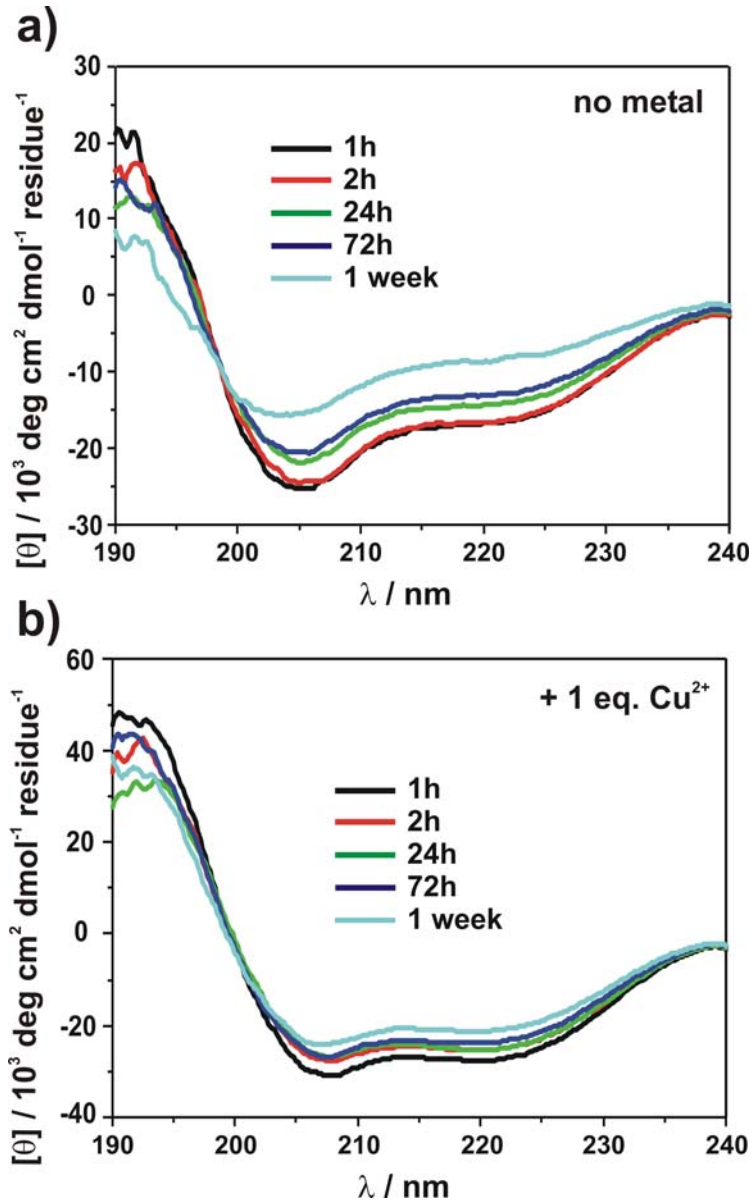


**Figure 8.21.** (a) CD spectra of peptide VW24 (*i,i+4*) in the absence of metal ions and (b) in presence of 1 eq.  $\text{Cu}^{2+}$  ( $c = 100\mu\text{M}$ , 10mM Tris / HCl, pH 7.4).

The direct precursor peptide VW17 adopted a clear helical conformation at pH 7.4 and a concentration of  $100\mu\text{M}$  (see section 7.2.5). In contrast, both His containing analogs VW23 and VW24 exhibit only a partially helical structure at these conditions (Figure 8.20a and Figure 8.21a). This slightly disturbed helical conformation obviously results from the His incorporation at central *heptad* repeat positions which are crucial for the coiled coil folding. However, the partially  $\alpha$ -helical conformation was retained for the entire observation period of one week, which indicates that no amyloids form at these conditions. This is in agreement with the folding behavior of VW17 and intent of the design.

Although both peptides exhibit a similar behavior in the absence of metal ions, distinct differences are observed in their presence. Peptide VW23 considerably unfolds after addition of one eq.  $\text{Cu}^{2+}$  and maintains an unordered conformation for one week. On the other hand,  $\text{Cu}^{2+}$  addition to peptide VW24 yields a predominantly  $\alpha$ -helical conformation which was likewise shown to be invariable for one week. Similar spectra have been obtained for lower peptide concentrations up to  $50\mu\text{M}$  (data not shown). Thus, metal binding to residues at  $i$  and  $i+2$  positions indeed disturbs the helical conformation, while metal coordination of His side chains at  $i$  and  $i+4$  positions stabilize the helical structure.

From these results, it can be concluded that the metal ion dependent stabilization or destabilization principles of the  $i,i+2$  and  $i,i+4$  strategy can be successfully applied for the coiled coil based model system. Only two Histidines are sufficient to determine the overall conformation of the 26 residue peptide and therefore provide a powerful tool for the design of metal ion sensitive amyloid forming model systems.

#### 8.2.4 VW25 and VW26

Based on the encouraging results of peptide VW23 and VW24 the next step was to implement the  $i,i+2$  and  $i,i+4$  strategy into the sequence of the basic amyloid forming coiled coil VW18. Figure 8.22 shows the sequence of the resulting peptides VW25 and VW26 as a helical wheel model and as an extended parallel and antiparallel  $\beta$ -sheet aligned in a zigzag fashion. The design of both peptides can be described by three general features: (I) All four positions governing the two coiled coil recognition motifs (a, d, e, and g) are optimized for a helical folding. Positions a and d are exclusively occupied by leucine residues. This ensures an efficiently packed hydrophobic core while positions e and g were designed to form exclusively attractive electrostatic interactions between the helices in the case of a parallel folding. (II) Analogous to VW18, three valine residues at the solvent exposed b, c and f positions enhance the system's intrinsic amyloid formation propensity. As described previously for VW23 and VW24, two of the Val residues at position 13 (b) and 14 (c) were rearranged to 20 (b) and 7 (c) to enable a His incorporation at central positions within the peptide sequence. (III) Metal coordinating His residues have been incorporated either at positions  $i$  and  $i+2$  to disrupt the helical structure or at positions  $i$  and  $i+4$  to stabilize the helical conformation upon the coordination of transition metal ions.

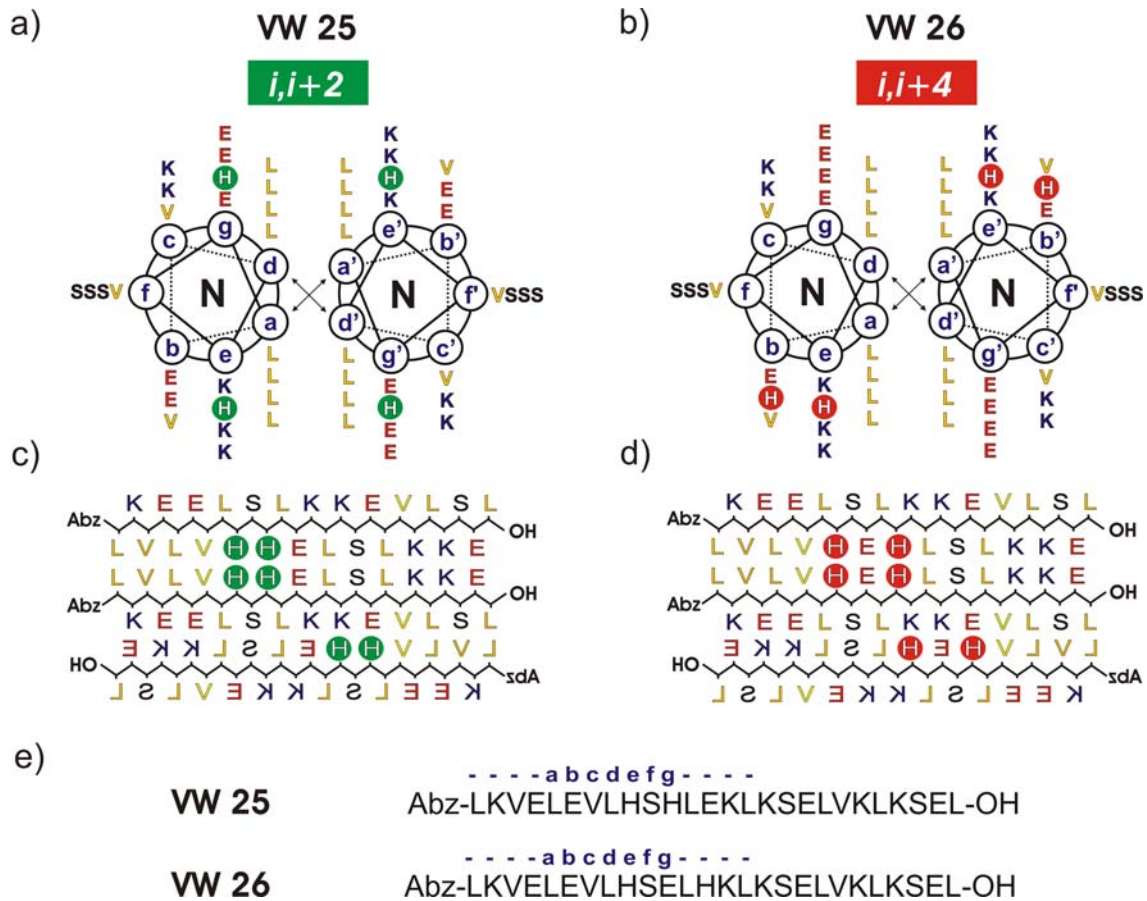


**Figure 8.22.** (a and b) Helical wheel diagram, (c and d) zigzag model of a parallel and an antiparallel  $\beta$ -sheet, as well as (e) sequence of peptides VW25 and VW26.

The impact of  $\text{Cu}^{2+}$  or  $\text{Zn}^{2+}$  binding on the conformation of both peptides was studied by CD spectroscopy after different times of incubation. Simultaneously, a ThT staining assay was performed to monitor the time dependent formation of amyloids. In the absence of metal ions, peptide VW24 exhibits a structural transition from a partially helical conformation to a  $\beta$ -sheet rich structure which is accompanied by slow precipitation (Figure 8.23a). This is in agreement with the VW18 based design and therefore indicates the slow association into amyloids at first glance. In contrast, addition of two equivalents of  $\text{Cu}^{2+}$  yields a perceptible content of random coil with spectra which were almost invariable for the entire observation period of 120h (Figure 8.23b). This effect was observed even more conspicuously at lower peptide concentrations (data not shown). Thus, the metal directed unfolding of the model system indeed appears to prevent the time dependent formation of amyloids. However, in presence of two eq. of  $\text{Zn}^{2+}$ , VW25 shows a different and completely unexpected behavior. Within minutes after  $\text{Zn}^{2+}$  addition unusually rapid precipitation occurred and ambiguous,  $\beta$ -sheet-like CD signatures were obtained (Figure 8.23c).

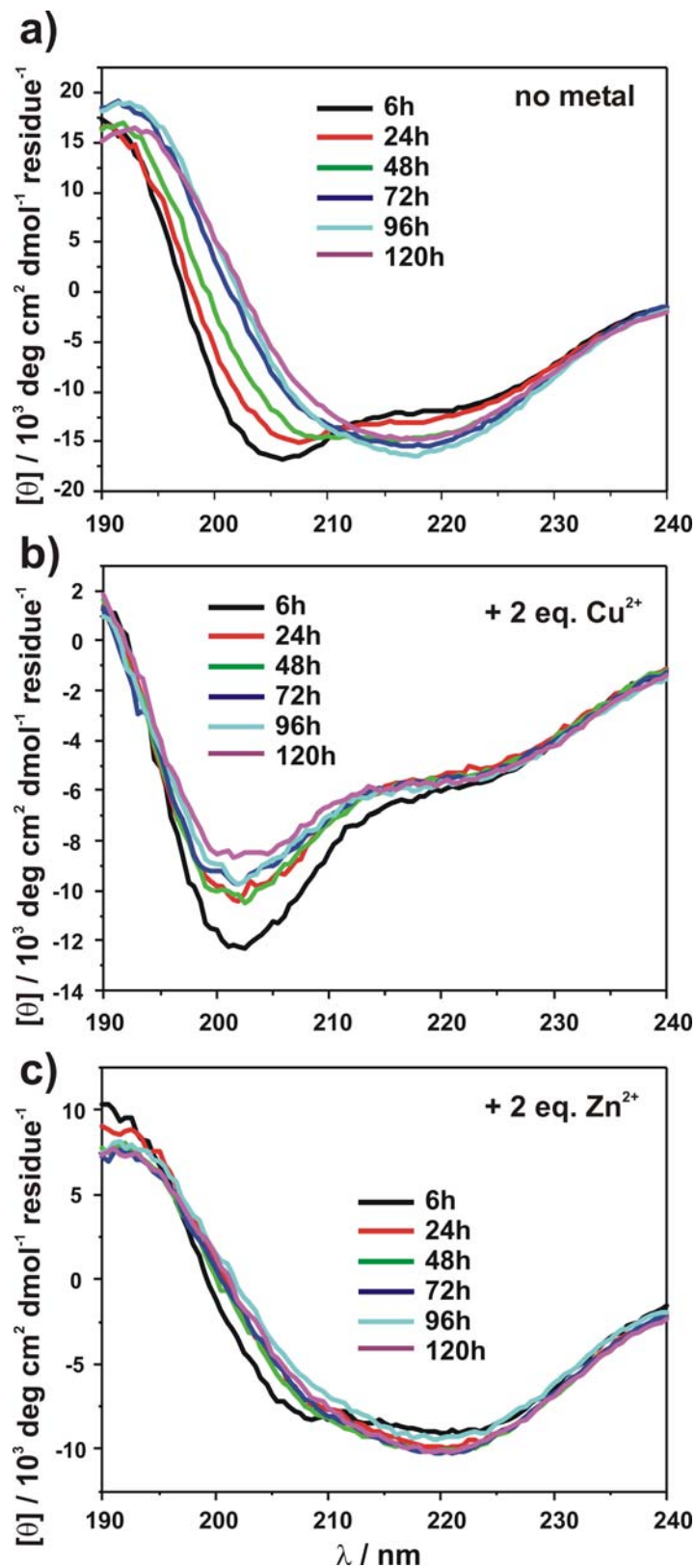


**Figure 8.23.** (a) CD spectra of peptide VW25 (*i,i+2*) in the absence of metal ions and (b and c) in presence of 2 eq.  $\text{Cu}^{2+}$  or  $\text{Zn}^{2+}$  ( $c = 100\mu\text{M}$ , 10mM phosphate buffer, pH 7.4).

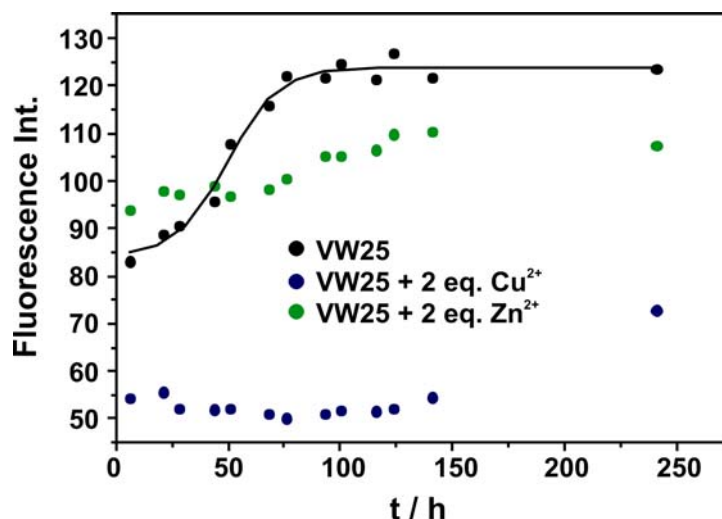


**Figure 8.24.** ThT assay of peptide VW25 (*i,i+2*) in the absence of metal ions (black) and in the presence of 2 eq. Cu<sup>2+</sup> (blue) or Zn<sup>2+</sup> (green) (50μM VW25, 50μM ThT, 10mM phosphate buffer, pH 7.4).

Since the results from the circular dichroism studies revealed a promising but partially inexplicit folding behavior, a ThT assay was performed to further substantiate the obviously different Cu<sup>2+</sup> and Zn<sup>2+</sup> dependent folding of VW25 (Figure 8.24). In the absence of metal ions, a typical sigmoidal increase in the ThT fluorescence was observed which further confirms the formation of amyloids. Interestingly, the relative fluorescence increase is five times lower than obtained for the non-His containing precursor peptide VW18. This indicates perceptible structural differences. Consequently, the suspicion arose that this effect resulted from the two shifted Val residues at position b and c, which might have caused a distinct structural arrangement within the fibrils. For the clarification of this issue, a new peptide termed VW28 was designed and characterized. The results are described in section 8.2.5. In contrast to VW25 in the absence of metal ions, addition of Cu<sup>2+</sup> as well as Zn<sup>2+</sup> did not yield a noticeably increased ThT fluorescence intensity.

Besides these spectroscopic investigations, an attempt was made to characterize the precipitating aggregates with cryo-TEM. Preliminary TEM experiments showed that, regardless if incubated with metal ions or not, VW25 forms sticky aggregates at elevated concentrations like those required for cryo-TEM. These cloggy bundles could only be diluted and dispersed with difficulties. Thus, detailed cryo-TEM investigations failed because of the irrepressible aggregation properties of the system. Consequently, it is still unclear, whether the Zn<sup>2+</sup> induced precipitation of VW25 is indeed accompanied by the formation of amyloids.

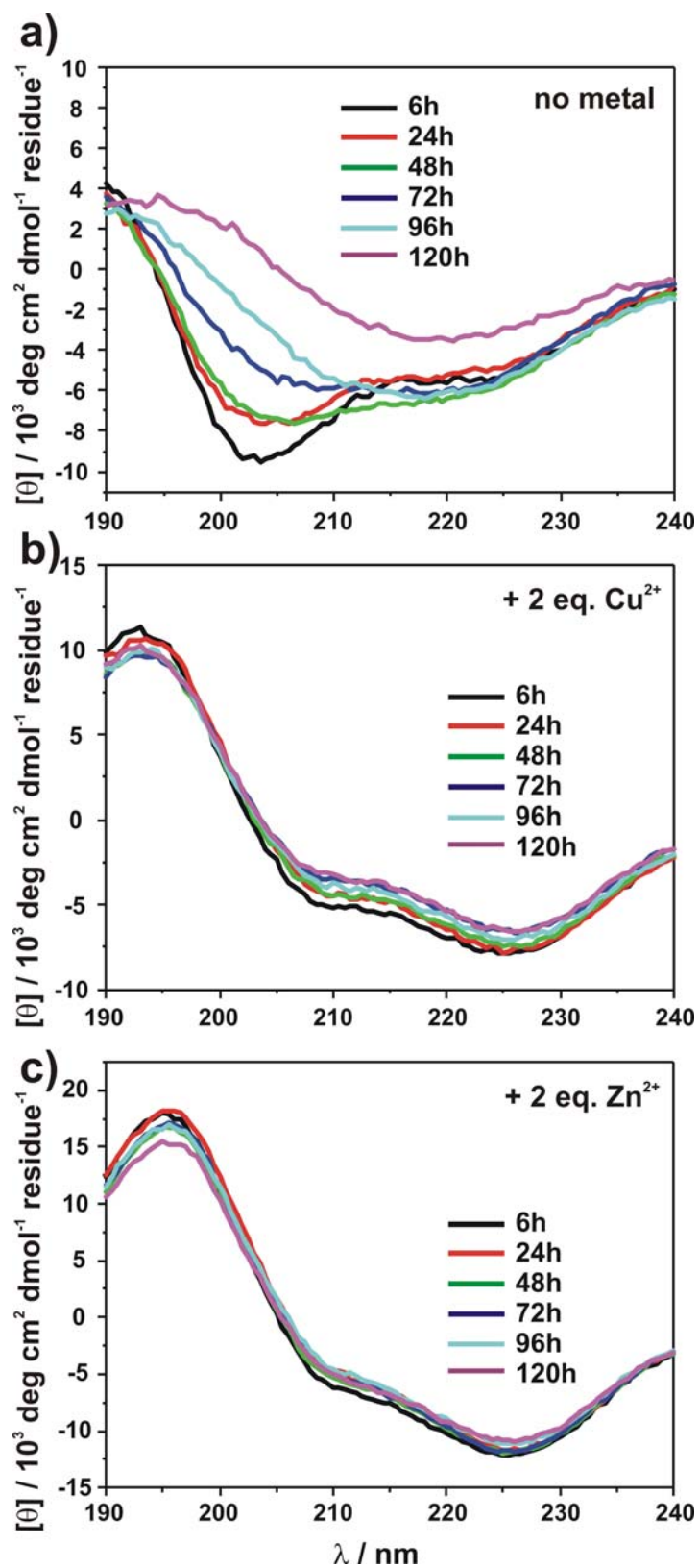


**Figure 8.25.** (a) CD spectra of peptide VW26 (*i,i+4*) in the absence of metal ions and (b and c) in presence of 2 eq.  $\text{Cu}^{2+}$  or  $\text{Zn}^{2+}$  ( $c = 100\mu\text{M}$ , 10mM phosphate buffer, pH 7.4).

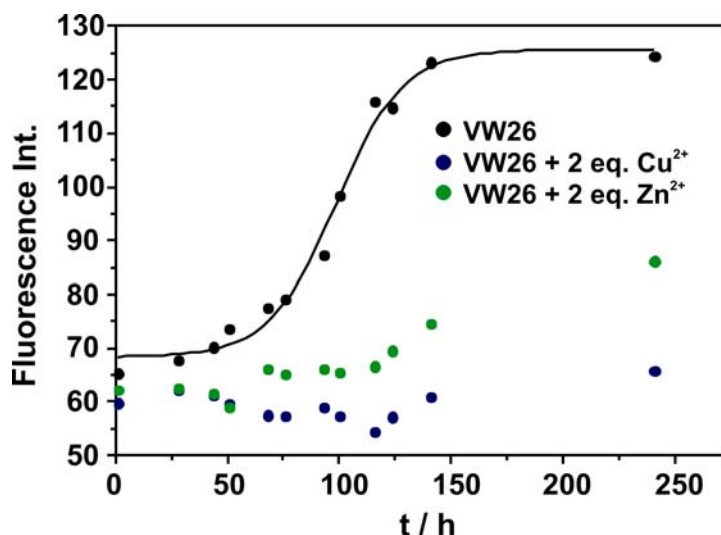


**Figure 8.26.** ThT assay of peptide VW26 (*i,i+4*) in the absence of metal ions (black) and in the presence of 2 eq.  $\text{Cu}^{2+}$  (blue) or  $\text{Zn}^{2+}$  (green) ( $50\mu\text{M}$  VW26,  $50\mu\text{M}$  ThT,  $10\text{mM}$  phosphate buffer, pH 7.4).

Unlike VW25, peptide VW26 exhibited a more explicit folding behavior. Figure 8.25 shows the CD spectra of VW26 in the absence of metal ions as well as in presence of two eq. of  $\text{Cu}^{2+}$  and  $\text{Zn}^{2+}$ . Without metal addition, a slow transformation from a partially helical structure to a  $\beta$ -sheet rich conformation was observed (Figure 8.25a). This structural transition is accompanied by a slow precipitation of aggregates which was expected for an amyloid association process and intent of the design. In presence of  $\text{Cu}^{2+}$  as well as  $\text{Zn}^{2+}$ , invariable  $\alpha$ -helical CD signatures with an increased relative ellipticity at 208nm were obtained for the complete observation period of 120h. Similar spectra were achieved for peptide VW19 at pH 7.4 (see section 8.1.3) and indicate the formation of large  $\alpha$ -helical assemblies. In contrast to VW19, which exhibited a gradual, time dependent  $\alpha$ -helical association, VW26 aggregates immediately after addition of the metal ion. Since  $\text{Cu}^{2+}$  as well as  $\text{Zn}^{2+}$  ions are able to bind more than one peptide strand, it appears likely that the formation of oligomeric peptide-metal complexes initiates the  $\alpha$ -helical aggregation process.

Based on these findings the question arose whether these  $\alpha$ -helical aggregates are non-amyloidogenic. To clarify this question a ThT assay was performed (Figure 8.26). Without metal addition a typical sigmoidal increase of the dye's fluorescence properties further confirms the association into amyloids. Contrarily, indistinct results are obtained in the presence of  $\text{Cu}^{2+}$  and  $\text{Zn}^{2+}$ . The ThT fluorescence intensity obviously remains unchanged, although a slight increase is observed after a long-term sample incubation of approx. 250h. Thus, the metal directed amyloid association presumably inhibits the

association into amyloids, but unfortunately ambiguous experimental results eliminate an explicit conclusion.

The experiments from the VW25 / VW26 peptide series, however, provide at least a basis for the further development of metal sensitive amyloid forming model peptides. Both peptides have been studied extensively and not all the data have been presented here. The observed folding and aggregation properties doubtlessly imply a certain feasibility for the integration of the  $i,i+2$  and  $i,i+4$  approach into a coiled coil based model system. Consequently, fine tuning of the models intrinsic amyloid formation properties was necessary for the design of a metal binding model system with a more explicit folding behavior. This attempt was successful and will be described in the two following subsections.

### 8.2.5 VW28

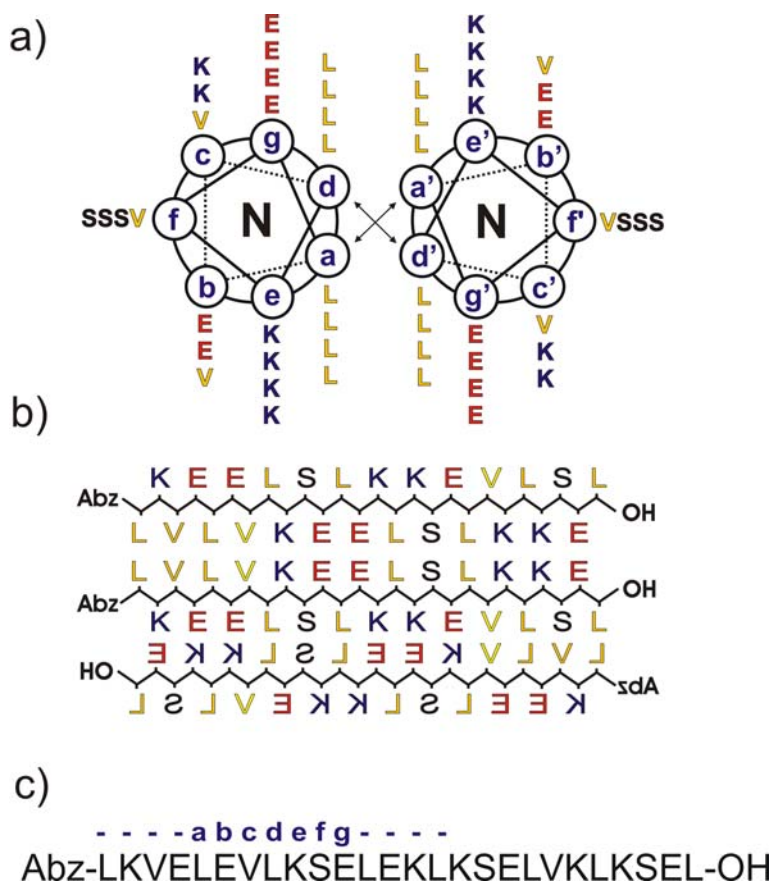


**Figure 8.27.** (a) Helical wheel diagram, (b) zigzag model of a parallel and an anti-parallel  $\beta$ -sheet, as well as (c) sequence of peptide VW27.

During the investigations on peptides VW25 and VW26 an unusually low response in the ThT assay was observed, even when the formation of  $\beta$ -sheet rich species was revealed by CD spectroscopy. Especially in comparison to the precursor peptide VW18, which showed an enormous increase of the ThT fluorescence, these results appeared incomprehensible. Thus, the suspicion arose, that the rearrangement of the two Val residues from *heptad* repeat positions 13 (b) and 14 (c) to position 20 (b) and 7 (c), respectively, has a paramount impact on the amyloid formation properties of the system. To substantiate this assumption, peptide VW28 was designed and characterized. Figure 8.27 shows the primary structure of VW28 as a helical wheel model and as an extended parallel and antiparallel  $\beta$ -sheet aligned in a zigzag fashion. Basically, the sequence resembles that of peptide VW18 with the exception of two Val residues that were shifted from position 13 (b) and 14 (c) to position 20 (b) and 7 (c), respectively.

The folding behavior of VW28 at pH 7.4 was monitored simultaneously by CD spectroscopy and a ThT staining assay (Figure 8.28 and Figure 8.29). Both methods doubtlessly reveal that VW28 forms amyloids with a conventional nucleation dependent pathway. The absolute ThT fluorescence increase, however, is distinctly lower than observed for VW18 (see section 7.2.6, Figure 7.21). Additionally, the amyloid association process is perceptibly decelerated. The ThT fluorescence inflection point of VW18 is reached after approx. 48h, while VW28 requires approx. 120h for 50% conversion. Thus, it can be concluded, that the position of the Val residues at *heptad* repeat positions b and c has a bigger impact than expected so far.

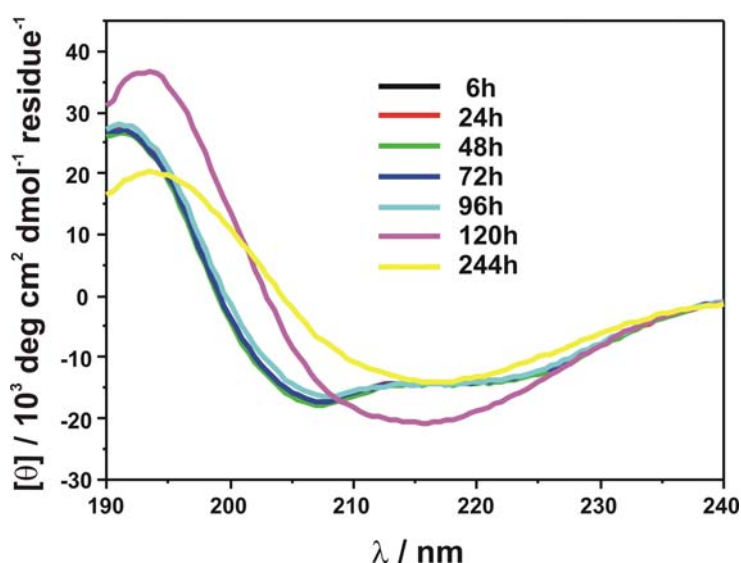


**Figure 8.28.** CD spectra of peptide VW28 at pH 7.4 after different incubation times ( $c = 95\mu\text{M}$ , 10mM phosphate buffer, pH 7.4).

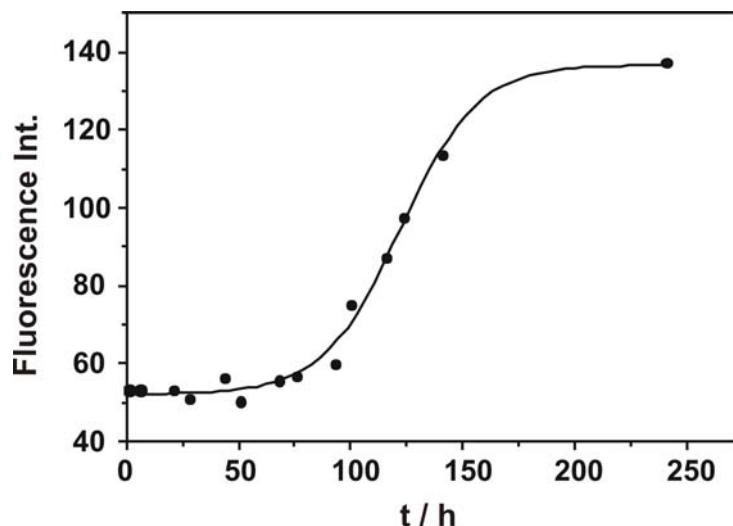


**Figure 8.29.** ThT assay of peptide VW28 (50 $\mu$ M VW28, 50 $\mu$ M ThT, 10mM phosphate buffer, pH 7.4).

Based on the differences between VW18 and VW28, further peptides with an altered Val positioning have been investigated.<sup>222</sup> In combination with previous experiments,<sup>223,227-229</sup> these data doubtlessly confirm that exclusively VW18 and VW18 related peptides such as VW19 exhibit this extraordinarily high amyloid formation tendency. Nevertheless, further experiments elucidating the internal structure within the protofilaments such as solid-state NMR are required for a molecular level understanding. Site-directed Pro mutagenesis might also provide valuable information on the location of  $\beta$ -strands within the primary structure of VW18.

### 8.2.6 VW29 and VW30

Further attempts regarding the implementation of the  $i,i+2$  and  $i,i+4$  strategy into the amyloid forming coiled coil model became self-evident from the comparison between VW18 and VW28. In principle, the design is similar to peptides VW25 and VW26, with the exception of the relative Val and His positioning (Figure 8.30). All three Val residues at the solvent exposed b, c, and f positions have been incorporated according to the design of VW18. The metal binding His residues were shifted by one *heptad* repeat, without changing their relative  $i,i+2$  or  $i,i+4$  arrangement, respectively. Analogous to the VW25 / VW26 peptide series, the design of VW29 and VW30 can be summarized to three key features: (I) Intact coiled coil interaction domains to ensure helical folding, (II) incorporation of three valine residues at b, c and f position to provide the

intrinsic amyloid formation propensity and (III) metal coordinating residues either at position  $i$  and  $i+2$  to destabilize the helical structure or at position  $i$  and  $i+4$  to stabilize the helical conformation upon the coordination of transition metal ions.

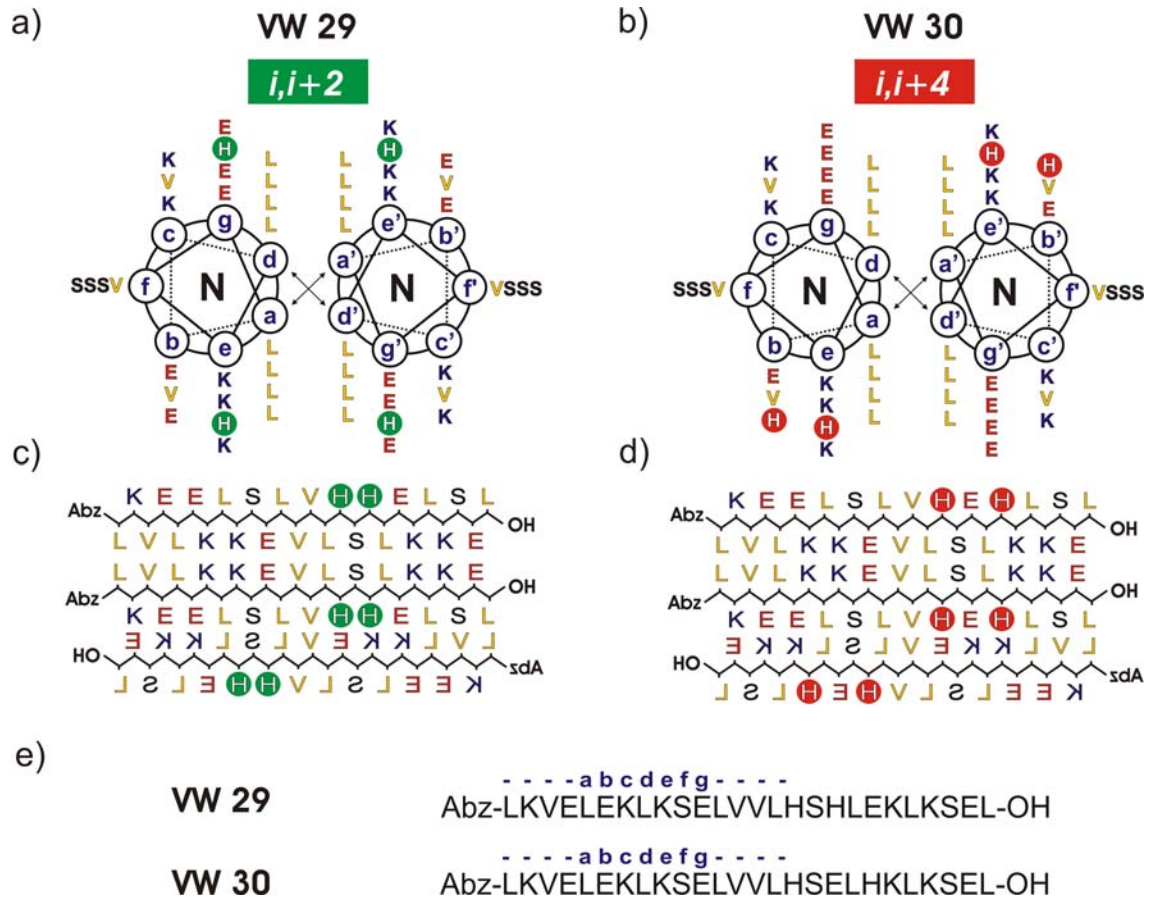


**Figure 8.30.** (a and b) Helical wheel diagram, (c and d) zigzag model of a parallel and an antiparallel  $\beta$ -sheet, as well as (e) sequence of peptides VW29 and VW30.

Both peptides were investigated by a battery of biophysical techniques. Not surprisingly, the metal ion dependent folding of VW29 and VW30 resembles the behavior of VW25 and VW26, although much more distinct structural effects were obtained. Figure 8.31 shows the CD spectra of peptide VW29 in the absence of metal ions as well as in presence of 2 eq.  $\text{Cu}^{2+}$  or  $\text{Zn}^{2+}$ . Starting with a partially helical conformation, VW29 slowly converts to a  $\beta$ -sheet rich structure within 120 hours in the absence of metal ions. This indicates a slow formation of amyloids. As expected, incubation with two equivalents of  $\text{Cu}^{2+}$  yielded random coil CD spectra, which were invariable for the entire observation period of ten days (data not shown). In contrast, addition of two equivalents of  $\text{Zn}^{2+}$  did not lead to unfolding and instead indicate an accelerated amyloid formation. A  $\beta$ -sheet rich conformation was observed within the first 100 hours.

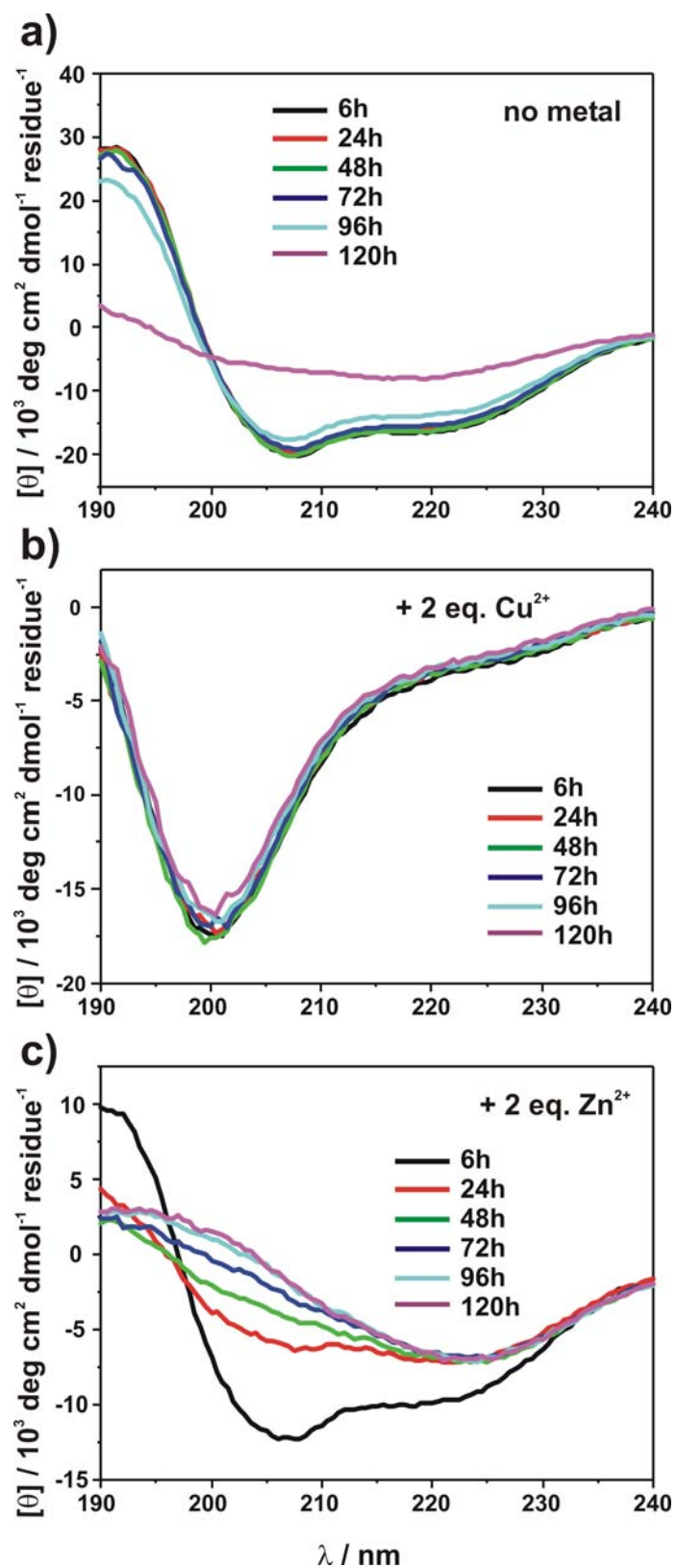


**Figure 8.31.** (a) CD spectra of peptide VW29 (*i,i+2*) in the absence of metal ions and (b and c) in presence of 2 eq.  $\text{Cu}^{2+}$  or  $\text{Zn}^{2+}$  ( $c = 100\mu\text{M}$ , 10mM phosphate buffer, pH 7.4).

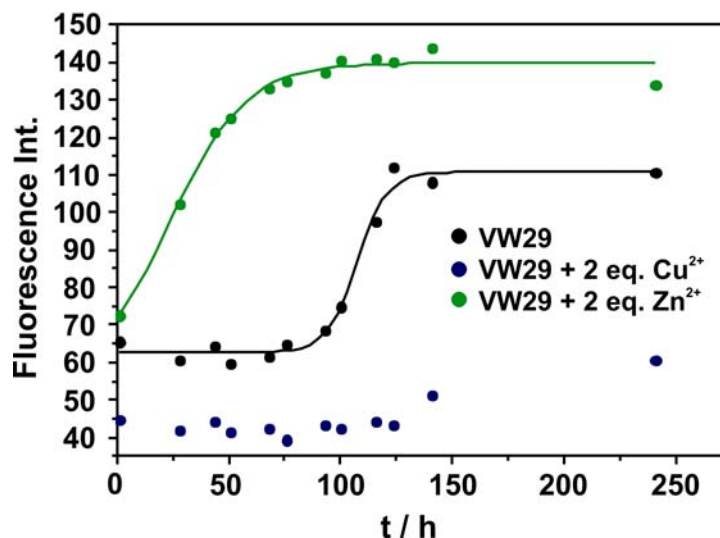
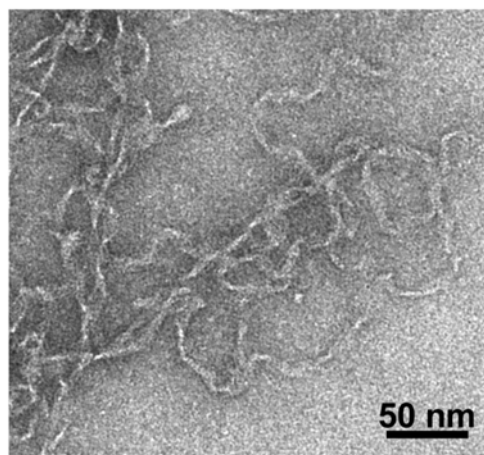


**Figure 8.32.** ThT assay of peptide VW29 (*i,i+2*) in the absence of metal ions (black) and in the presence of 2 eq.  $\text{Cu}^{2+}$  (blue) or  $\text{Zn}^{2+}$  (green) ( $50\mu\text{M}$  VW29,  $50\mu\text{M}$  ThT,  $10\text{mM}$  phosphate buffer, pH 7.4).

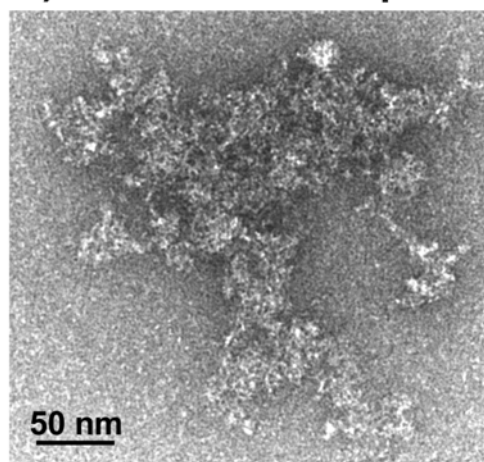
A ThT staining assay confirmed the observed differences between  $\text{Cu}^{2+}$  and  $\text{Zn}^{2+}$  (Figure 8.32). Without metal addition, a sigmoidal increase of the dye's fluorescence intensity was observed which points to the typical pathway of a nucleation dependent amyloid elongation process. Not surprisingly,  $\text{Cu}^{2+}$  addition yielded almost unchanged fluorescence intensities and, thus, supports the CD spectroscopic observations of a random coil conformation. As already assumed from the CD spectra, addition of  $\text{Zn}^{2+}$  leads to an accelerated amyloid formation as indicated by a rapid increase of the ThT fluorescence intensity.

In order to clarify the different amyloid formation tendencies observed by spectroscopy, the resulting peptide aggregates were characterized by TEM after incubation of seven days. To overcome the dilution and dispersion difficulties that occurred at early cryo-TEM studies on VW25, negative staining in combination with lower concentrated samples was employed. In the absence of metal ions, peptide VW29 forms fibrils with either long straight and/or flexible ribbon morphology (Figure 8.33a). Contrarily, in presence of  $\text{Cu}^{2+}$ , aggregates possess an amorphous morphology, thus emphasizing the occurrence of unfolded species (Figure 8.33b). Consistent with the spectroscopic data,  $\text{Zn}^{2+}$  addition yields ribbon-like amyloid fibers similar to those observed in the absence of metal ions (Figure 8.33c).

a) no metal



b) + 2eq.  $\text{Cu}^{2+}$



c) + 2eq.  $\text{Zn}^{2+}$

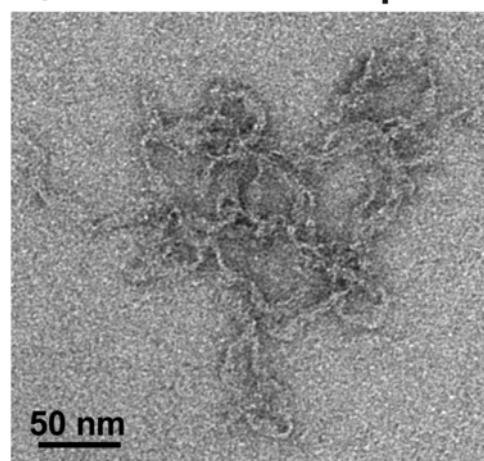


**Figure 8.33.** (a) Negative staining TEM micrographs of peptide VW29 (*i,i*+2) in the absence of metal ions and (b and c) in presence of 2 eq.  $\text{Cu}^{2+}$  or  $\text{Zn}^{2+}$  ( $c = 100\mu\text{M}$ , 10mM phosphate buffer, pH 7.4, one week incubation).

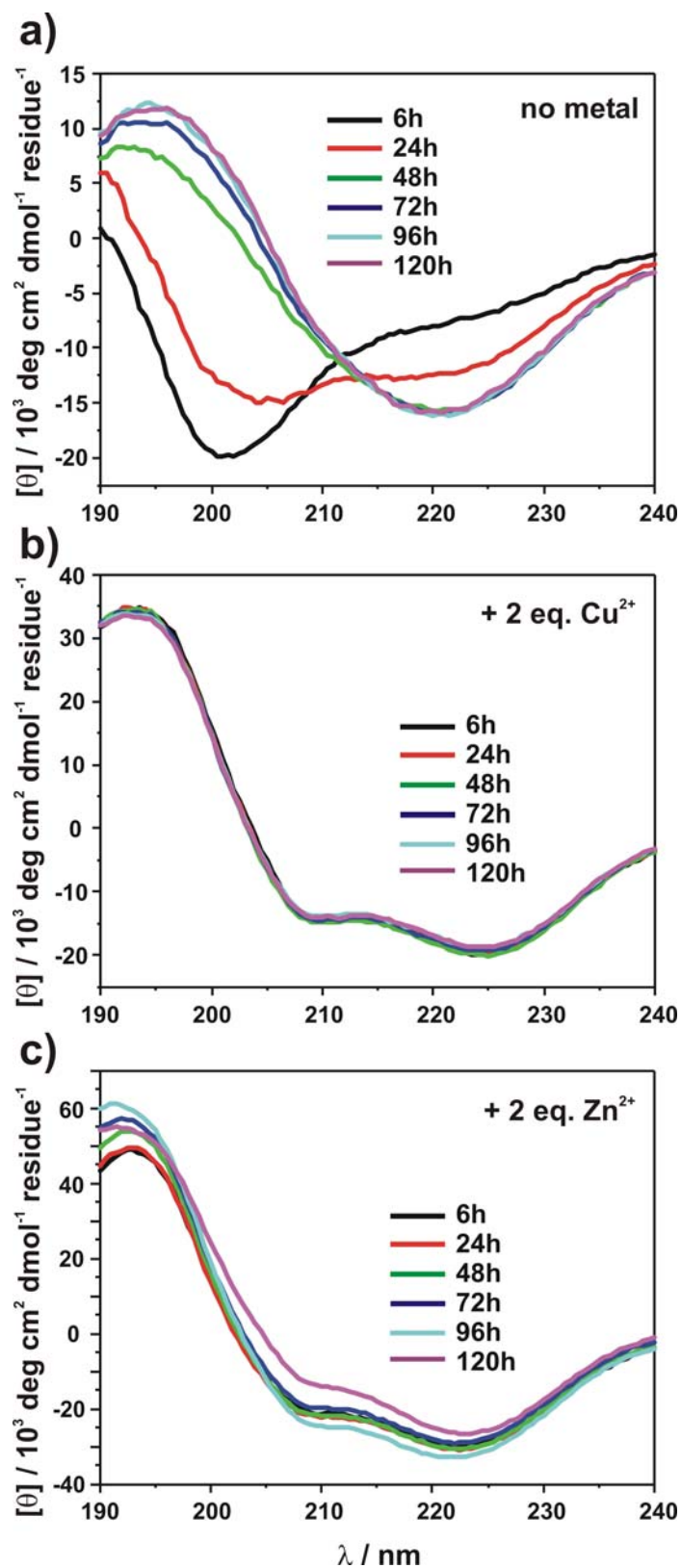


**Figure 8.34.** (a) CD spectra of peptide VW30 ( $i,i+4$ ) in the absence of metal ions and (b and c) in presence of 2 eq.  $\text{Cu}^{2+}$  or  $\text{Zn}^{2+}$  ( $c = 100\mu\text{M}$ , 10mM phosphate buffer, pH 7.4).

In contrast to peptide VW29, peptide VW30 does not discriminate in secondary structure formation upon coordination to  $\text{Cu}^{2+}$  or  $\text{Zn}^{2+}$ . In the absence of metal ions, peptide VW30 rapidly converts from a mainly unfolded state to a  $\beta$ -sheet, which indicates a fast amyloid formation (Figure 8.34a). Addition of either  $\text{Cu}^{2+}$  or  $\text{Zn}^{2+}$  yields helical structures which were retained for the entire observation period of ten days (Figure 8.34b and c). Staining of the resulting aggregates with ThT confirmed the CD data. Without metal addition a strong increase in the dyes fluorescence was observed, while samples incubated with  $\text{Cu}^{2+}$  or  $\text{Zn}^{2+}$  did not show any increase in the fluorescence intensity (Figure 8.35). Thus, addition of metal ions to VW30 shifts the equilibrium to the helical conformation and, as a result, inhibits the amyloid formation process.

Furthermore, TEM measurements of the resulting aggregates after seven days of incubation revealed distinct morphological differences. In the absence of metal ions, peptide VW30 typically forms twisted fibrils containing four or more protofilaments (Figure 8.36a). Additionally, twisted ribbons as well as tubular assemblies were found at these conditions (data not shown).<sup>247</sup> These results support the spectroscopic observations of a classical amyloid formation process. In contrast, samples incubated with  $\text{Cu}^{2+}$  as well as  $\text{Zn}^{2+}$  did not show aggregates with a fibrous morphology as would be expected for amyloids. In the presence of  $\text{Cu}^{2+}$ , short and sticky rod-like assemblies have been found while  $\text{Zn}^{2+}$  addition yielded cloggy bundles of bended rods (Figure 8.36b and c).

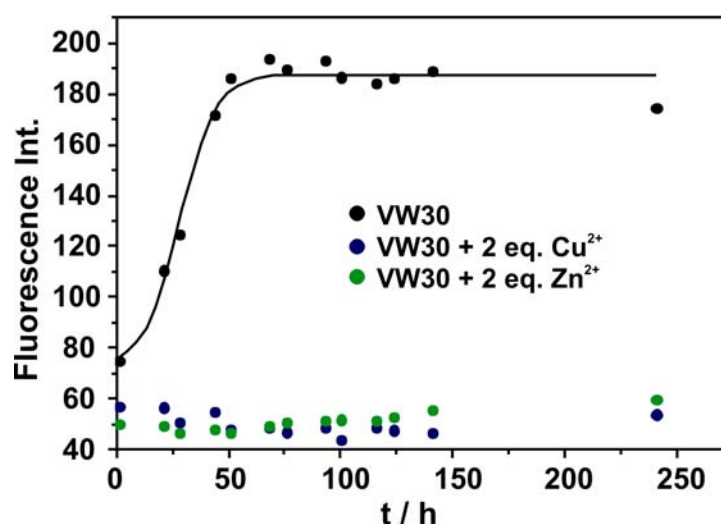


**Figure 8.35.** ThT assay of peptide VW30 ( $i,i+4$ ) in the absence of metal ions (black) and in the presence of 2 eq.  $\text{Cu}^{2+}$  (blue) or  $\text{Zn}^{2+}$  (green) ( $50\mu\text{M}$  VW30,  $50\mu\text{M}$  ThT,  $10\text{mM}$  phosphate buffer, pH 7.4).

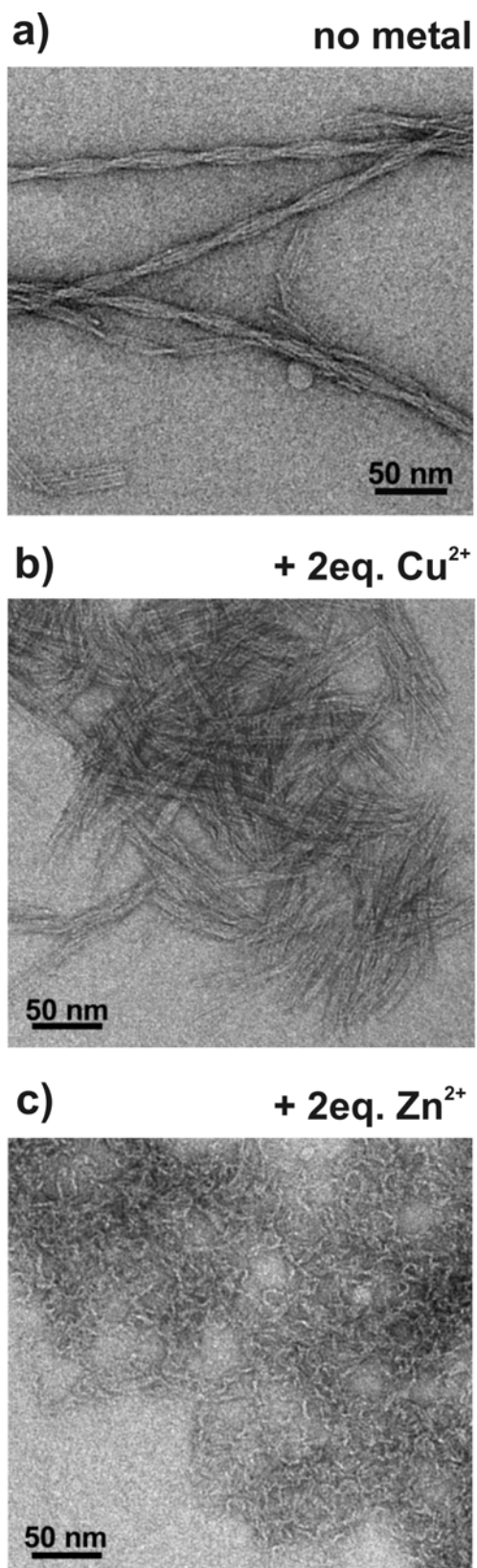


**Figure 8.36.** (a) Negative staining TEM micrographs of peptide VW30 (*i,i+4*) in the absence of metal ions and (b and c) in presence of 2 eq.  $\text{Cu}^{2+}$  or  $\text{Zn}^{2+}$  ( $c = 100\mu\text{M}$ , 10mM phosphate buffer, pH 7.4, one week incubation).

Although peptide VW30 exhibits a similar  $\alpha$ -helical CD signature and non-amyloidogenic behavior in the presence of  $\text{Cu}^{2+}$  and  $\text{Zn}^{2+}$ , the resulting aggregates are distinctly different. The different coordination geometry of  $\text{Cu}^{2+}$  and  $\text{Zn}^{2+}$  certainly contributes to the aggregate morphology.  $\text{Zn}^{2+}$  usually prefers a coordination number of four with tetrahedral geometry. In contrast, many cysteine free  $\text{Cu}^{2+}$  proteins, so-called type 2  $\text{Cu}^{2+}$  proteins, mainly possess a coordination number of four but with a square planar arrangement.<sup>230,248,249</sup> Electron Paramagnetic Resonance (EPR) experiments have been performed to shed light on the geometry of the presented peptide- $\text{Cu}^{2+}$  complexes and to clarify whether a type 2  $\text{Cu}^{2+}$  center is present.

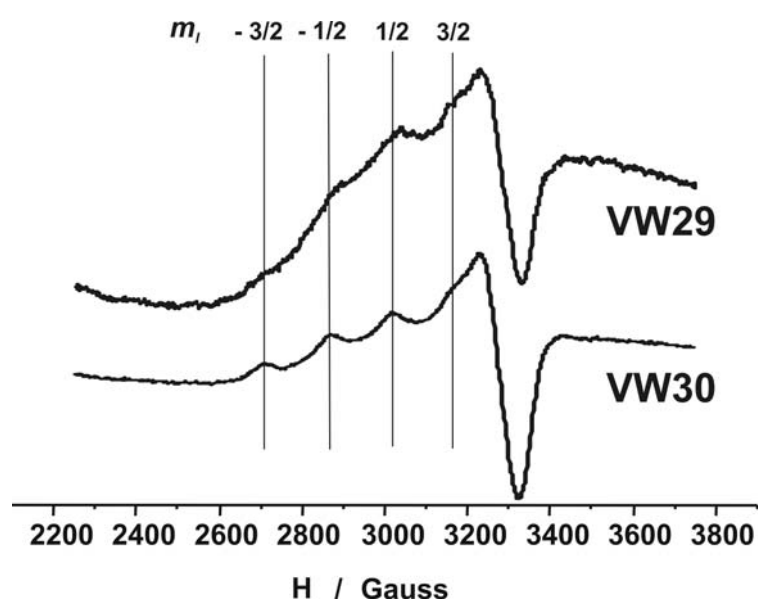


**Figure 8.37.** X-band EPR spectra of freshly prepared VW29 and VW30  $\text{Cu}^{2+}$  complexes. ( $c \sim 1\text{mM}$ ,  $2\text{mM Cu(OAc)}_2$ ,  $10\text{mM phosphate buffer}$ ,  $\text{pH } 7.4$ ,  $10\% \text{ glycerol (v,v)}$ ,  $T = 130\text{K}$ ). The following parameters have been determined. VW29:  $g_{\parallel} = 2.272$ ,  $A_{\parallel} = 154 * 10^{-4}\text{cm}^{-1}$ ,  $g_{\perp} = 2.060$ . VW30:  $g_{\parallel} = 2.284$ ,  $A_{\parallel} = 158 * 10^{-4}\text{cm}^{-1}$ ,  $g_{\perp} = 2.063$ . (Exp. errors:  $g_{\perp} \pm 0.003$ ,  $A_{\parallel} \pm 3 * 10^{-4}\text{cm}^{-1}$ ).

Figure 8.37 shows X-band EPR spectra of  $\text{Cu}^{2+}$  ions bound to peptide VW29 and VW30. In order to minimize the EPR signal of aqueous  $\text{Cu}^{2+}$  ions,  $\text{Cu(OAc)}_2$  was used, since it forms dimers in frozen solution. The Cu-Cu dimer EPR spectrum is well known<sup>250</sup> but has not been observed during the described measurements. Thus, the obtained signal exclusively arises from peptide-bound  $\text{Cu}^{2+}$ . Both spectra show a typical  $\text{Cu}^{2+}$  hyperfine splitting with characteristic  $g_{\parallel}$  (the parallel component of the axially symmetric  $g$  tensor) and  $A_{\parallel}$  (the parallel component of the hyperfine interaction) values,

indicating the presence of a type 2  $\text{Cu}^{2+}$  center in a mixed nitrogen/oxygen environment.<sup>251</sup> Similar spectra have been obtained for naturally occurring amyloids such as Alzheimer's Amyloid  $\beta$ ,  $\alpha$ -synuclein and prion proteins.<sup>68,252-255</sup> From the obtained values a 2N/2O or 3N/1O coordination environment can be proposed, since lower  $g_{\parallel}$  and higher  $A_{\parallel}$  values would be expected for 4N binding.<sup>68</sup> As a result, it appears likely that both His residues within one peptide strand bind to  $\text{Cu}^{2+}$  with almost square planar geometry, which supports the structure inducing effect of the peptide-metal coordination.  $^{14}\text{N}$  hyperfine splittings which would be helpful for the interpretation could not be resolved.

In summary, the implementation of the  $i,i+2$  and  $i,i+4$  strategy into the primary structure of peptide VW18 in the end succeeded to generate a series of amyloid forming model peptides that sensitively react on the presence of transition metal ions. Both peptides - VW29 as well as VW30 - form amyloids within days the absence of metal ions. Regardless of the His positions, coordination of  $\text{Cu}^{2+}$  throughout inhibits the formation of amyloids by either metal directed unfolding (VW29) or helix stabilization (VW30). In contrast, the presence of  $\text{Zn}^{2+}$  was shown to accelerate the amyloid formation if two metal binding sites are placed one residue apart from each other (VW29) and thus, point to the opposite side of the helical cylinder.  $\text{Zn}^{2+}$  binding to peptide VW30, where both metal binding residues are adjacent towards each other at the helical cylinder, shows a similar amyloid inhibiting and helix-inducing behavior as observed for  $\text{Cu}^{2+}$ . Thus, it can be concluded that metal binding accomplishes inhibition or acceleration of the amyloid formation process by either stabilization or destabilization of a competitive conformation.

The accelerated amyloid formation of peptide VW29 in the presence of  $\text{Zn}^{2+}$  can be explained by the position of the His residues in case of  $\beta$ -sheet folding. Extended  $\beta$ -strands in general possess a zigzag alignment. As a result, the His residues at  $i$  and  $i+2$  positions would be presented in close proximity towards each other at the same side of the strand and can therefore be easily accessed by metal ions. However, His at  $i$  and  $i+4$  position would be presented at the same side of the  $\beta$ -strand as well, but their side chains are located far apart from each other, thus preventing an efficient metal coordination. Therefore, it appears likely that only metal binding to residues at positions  $i$  and  $i+2$  has the potential to induce and stabilize amyloids and their  $\beta$ -sheet rich precursors.

More importantly, the results indicate that the nature of the metal ion also significantly contributes to the amyloid formation process. Interestingly, the behavior of peptide VW29 impressively resembles the  $\text{Cu}^{2+}$  and  $\text{Zn}^{2+}$  dependent amyloidogenesis of Alzheimer's  $\text{A}\beta$  *in vitro*. Recently, Saxena and co-workers<sup>253</sup> showed that binding of high concentrations of  $\text{Cu}^{2+}$  to  $\text{A}\beta$  yields granular non-amyloidogenic aggregates, while Lynn and co-workers<sup>66</sup> reported the accelerating effect of  $\text{Zn}^{2+}$  binding on the amyloid formation process. Moreover, Stellato et al. determined perceptible differences in the stoichiometry and coordination geometry of  $\text{A}\beta_{(1-40)}\text{-Cu}^{2+}$  and  $\text{Zn}^{2+}$  complexes obtained from resuspended fibrils.<sup>256</sup> Model peptide VW29 is a completely artificial, *de novo* designed molecule and does not possess any sequence homologies to  $\text{A}\beta$ , even in terms of the His positions. However, it shows a similar behavior of an inhibited amyloid formation in the presence of  $\text{Cu}^{2+}$  and an accelerated amyloid association in the presence of  $\text{Zn}^{2+}$ . Consequently, it can be reasoned that the intrinsic binding characteristic of the particular metal ion has a greater impact on amyloid formation than accepted so far. It is still unclear, how many peptide strands bind to the  $\text{Cu}^{2+}$  or  $\text{Zn}^{2+}$  center of the presented peptide-metal complexes. Thus, further studies on the peptide/metal stoichiometry are needed to gain structural knowledge of the metal's coordination sphere.